

Hamiltonian cycles on Ammann-Beenker Tilings

Shobhna Singh,^{1,*} Jerome Lloyd,² and Felix Flicker^{1,3}

¹*School of Physics and Astronomy, Cardiff University,
The Parade, Cardiff CF24 3AA, United Kingdom*

²*Department of Theoretical Physics, University of Geneva,
24 rue du Général-Dufour, 1211 Genève 4, Switzerland*

³*School of Physics, H. H. Wills Physics Laboratory,
Tyndall Avenue, Bristol, BS8 1TL, United Kingdom*

We provide a simple algorithm for constructing Hamiltonian graph cycles (visiting every vertex exactly once) on the set of aperiodic two-dimensional Ammann-Beenker (AB) tilings. Using this result, and the discrete scale symmetry of AB tilings, we find exact solutions to a range of other problems which lie in the complexity class NP-Complete for general graphs. These include the equal-weight travelling salesperson problem, providing for example the most efficient route a scanning tunneling microscope tip could take to image the atoms of physical quasicrystals with AB symmetries; the longest path problem, whose solution demonstrates that collections of flexible molecules of any length can adsorb onto AB quasicrystal surfaces at density one, with possible applications to catalysis; and the 3-colouring problem, giving ground states for the q -state Potts model ($q \geq 3$) of magnetic interactions defined on the planar dual to AB, which may provide useful models for protein folding.

I. INTRODUCTION

Fractal geometric loop structures are ubiquitous in physics, appearing often as the natural degrees of freedom in models of critical phenomena. Examples include the fluctuating domain walls of an Ising magnet, the compact shapes of long polymer chains [1], or the space-time trajectories of quantum particles. A special class of loops, attracting much attention beyond physics, are the Hamiltonian cycles. A Hamiltonian cycle of a graph is a closed, self-avoiding loop that visits every vertex precisely once. Study of these objects dates at least to the 9th century CE, when the Indian poet Rudraṭa constructed a poem based on a ‘Knight’s tour’ of the chessboard. Since then they have appeared in a variety of applications in the sciences and mathematics including protein folding [2, 3], traffic models, spin models in statistical mechanics [4, 5], and ice-type models of geometrically frustrated magnetism [6, 7].

Hamiltonian cycles have been used to model the statistics of polymer melts [1, 8–10]: for example, the critical scaling exponents were calculated for polymer chains in 2D using the self-avoiding walk on the honeycomb lattice [11, 12]. They have also played a key role in the study of protein folding [1, 2, 13–16]. The shapes (‘conformational properties’) of proteins play a significant role in their biological function. Proteins often adopt remarkably compact and symmetrical structures compared to the more general class of polymers [14]. A key question is how to predict 3D conformational properties from the 1D sequences of amino acids from which the proteins are built. One route is to study ‘simple exact models’ in which the amino acids are represented by structureless

units, each occupying the vertex of a graph. Neighbouring units in the protein must be nearest neighbours on the graph. The graphs are chosen to have specific geometrical embeddings, typically periodic lattices. While not providing accurate geometrical models, such approaches have the advantage of being exactly solvable. They are also able to capture ‘non-local’ interactions, in which amino acids interact when they are neighbours on the graph but not on the 1D chain itself [1, 9, 13, 17, 18]. Remarkably, 2D graphs often give qualitatively similar results to 3D graphs while affording a significant computational advantage [14]. Simple exact models have also been instrumental in the development of polymer physics more generally [8, 19–22].

The $O(n)$ model in statistical physics, which describes n -component spins interacting with their nearest lattice neighbours with isotropic couplings [4, 5], can be mapped to a problem involving self-avoiding loops [17, 23]. The probability of a given loop configuration is weighted according to two fugacities: x weighting the total perimeter of the loops, and n the number of loops. The $O(n)$ phase diagram encapsulates many well-known models in statistical physics. For example, the ferromagnetic Ising model arises for $n = 1$, where the loops represent the domain walls in the low temperature limit (thus the Ising spins are defined on the planar dual lattice), while in the high temperature limit the natural degrees of freedom are again loops, though their expression in terms of the original spin variables is less intuitive; the q -state Potts models can be related to the $n = \sqrt{q}$ limit; as $x \rightarrow \infty$ every lattice site is visited by a loop and one arrives at the so-called ‘fully-packed loop’ (FPL) models, which additionally model crystal surface growth; and in the $x \rightarrow \infty, n \rightarrow 0$ limit, the system is forced into a single macroscopic loop traversing every site of the system, which is a Hamiltonian cycle [23, 24]. Studying Hamiltonian cycles can thus lead to an understanding of

* shobhna862@gmail.com

a variety of other AB models in a given system, and for this reason a great deal of work has been put into their study – primarily in the simplest context of periodic regular lattices [5, 9, 11, 17, 18, 24–37]. Given, however, that the complex fractal structures (e.g. polymer/protein structures) these objects aim to model often lack translational symmetry and favour disordered growth [38], studies of Hamiltonian cycles in settings where translational symmetry is absent may unearth important clues towards the universality of these results.

In this paper we present a simple algorithm for constructing Hamiltonian cycles and fully packed loops on a set of infinite graphs which do not admit periodic planar embeddings. Specifically, we consider graphs formed from the edges and vertices of Ammann-Beenker (AB) tilings (Fig. 1). These are two-dimensional (2D) infinite aperiodic tilings [39–41] built from two tiles, a square and a rhombus. They lack the translational symmetry of periodic lattices but nevertheless feature long-range order on account of a discrete scale invariance [42], evidenced by sharp spots in their diffraction patterns [40, 43, 44]. The long-range order of AB enables exact analytical results to be proven, while their infinite extent allows consideration of the thermodynamic limit of an infinite number of vertices, of interest in condensed matter physics where physical quasicrystals are known which with the symmetries of AB [45, 46]. Recent experiments have demonstrated tunable quasicrystal geometries in twisted trilayer graphene [47], while 8-fold symmetric structures have also been created in optical lattices [48, 49]. Quasicrystals host a broad range of exciting physical phenomena from exotic criticality [50, 51] to charge order [52, 53] to topology [53–55], with the lack of periodicity often leading to novel behaviours.

Efficient Hamiltonian cycle constructions exist for certain special classes of graph [56–58]. One example is 4-connected planar graphs, defined as requiring the deletion of at least 4 vertices to disconnect them [59]. This result was recently employed in the elegant design of ‘quasicrystal kirigami’ [60] using a construction based on Hamiltonian cycles defined on the planar dual to AB. However, to our knowledge AB tilings themselves are not covered by any such special case (they are for example 3-connected). The unexpectedness of AB tilings’ admittance of Hamiltonian cycles can be seen by comparison to rhombic Penrose tilings, which are in many ways similar to AB. These, too, are a set of infinite 2D tilings built from two tile types (two shapes of rhombus); they are again aperiodic but long-range ordered; and the resulting graphs are bipartite, meaning the vertices divide into two sets such that vertices in one set connect only to vertices in the other – another property shared with AB. Yet Penrose tilings cannot admit Hamiltonian cycles, because they do not admit perfect dimer matchings (sets of edges such that each vertex meets precisely one edge) [61]. The latter is a necessary condition for the former, since deleting every second edge along a Hamiltonian cycle results in a perfect matching. It is difficult

to think of any special case which could cover AB which would not also cover Penrose tilings.

The difficulty of constructing Hamiltonian cycles in arbitrary graphs can be made precise using the notion of computational complexity. Given a graph, the question of whether it admits a Hamiltonian cycle lies in the complexity class ‘non-deterministic polynomial time complete’ (NPC) [62, 63]. These problems are prohibitively hard to solve – the fastest known exact algorithms scale exponentially – but a given solution can be checked quickly, in polynomial time (P). ‘Completeness’ refers to the fact that if a polynomial-time algorithm were found which solved any NPC problem, all problems in the broader class NP would similarly simplify. Loosely, all problems in NP contain a bottleneck in NPC.

We do not purport to solve an NPC problem. Rather, we show that AB is a previously unknown special case of the Hamiltonian cycle problem which lies in P rather than NPC. As such, it does not follow that all NP problems can be solved in polynomial time on AB. However, we might reasonably hope that our Hamiltonian cycles permit new solutions to certain problems on AB, and indeed we find that this is the case. Using both the Hamiltonian cycles and the inherited discrete scale symmetry of AB tilings, we find exact solutions on AB to a range of other non-trivial problems which are NPC in general graphs [63]. We present three cases which have important applications to physics.

For example, by solving the ‘equal-weight travelling salesperson problem’ (Sec. IV A) on AB we provide a maximally efficient route for a scanning tunneling microscopy (STM) tip to follow in order to scan every atom on the surface of an AB quasicrystal in a given area. Given that a state of the art STM measurement might take of order a month, such efficient routes are highly desirable. The problem of finding them is not present in periodic crystals, where efficient routes can be found by following crystal symmetries.

By solving the ‘longest path problem’ (Sec. IV B) on AB we identify the longest possible path visiting every site within a given region. This shows that long, flexible molecules, such as polymers, can adsorb onto the surface of AB quasicrystals with maximal efficiency. Moreover, by breaking the longest path into smaller units, our solution demonstrates that collections of flexible molecules of arbitrary lengths can also adsorb at maximal packing density. This has potential applications to catalysis, in which the activation energy of a reaction between molecules is lowered by having them adsorb onto a surface. Quasicrystal surfaces are emerging as an interesting material for adsorption because they provide different local environments with a range of bond angles [64], in contrast to the periodic surfaces of crystals. They have potential applications in hydrogen adsorption and storage [65, 66], low friction machine parts, and non-stick coatings [65, 67].

The ‘three colouring problem’ asks whether it is possible to colour the tiles of a planar tiling with three colours

such that no two tiles sharing an edge share a colour [68]. We solve this problem on AB in Sec. IV C. The three colours can represent the degrees of freedom in the three-state Potts model of nearest neighbour magnetic interactions. The three-coloured AB tiling thereby gives an unfrustrated ground state for the antiferromagnetic q -state Potts model, with spins defined on the faces of AB, for any $q \geq 3$.

The Potts model was originally introduced to describe interactions between magnetic ions [68, 69], gaining relevance to quasicrystals with the discovery of ordered magnetic states in these materials [70–74]. More recently it, too, has been used as a simple model of protein folding, with Potts variables representing the q species of amino acid comprising the protein chain [3, 75, 76]. The interaction between amino-acids can be either repulsive or attractive depending on the solvent which surrounds the protein. Compared to the typical approximation that the protein folds on a square lattice [1, 9, 76], AB arguably defines a better approximation to the real problem, in which the amino acids have continuous spatial degrees of freedom. This is because AB has a larger range of bond angles, better approximating a continuous rotational symmetry than any 2D regular lattice.

In Appendix B we solve a further three problems, on AB, which are known to be NPC in general graphs: the minimum dominating set problem (Sec. B 1); the domatic number problem (Sec. B 2); and the induced path problem (Sec. B 3). Doubtless many more examples can be found. The fact that many NPC problems admit polynomial-time solutions on AB suggests that the discrete scale symmetry of quasiperiodic lattices may be as powerful a simplifying factor as the discrete translational symmetry widely used to obtain exact results on periodic lattices.

The remainder of this paper is organized as follows. We introduce the necessary background on the AB tilings and graph theory in Sec. II. In Sec. III we prove the existence of Hamiltonian cycles on the AB tiling, proving along the way the possibility of fully packed loops, and give details of our algorithm. In Sec. IV we utilise the approach to present exact solutions, on AB, to three problems which are NPC for general graphs: the equal-weight travelling salesperson problem (Sec. IV A); the longest path problem (Sec. IV B); and the three-colouring problem (Sec. IV C). We comment on the applications for each. In Appendix B we provide exact solutions to three other problems on AB: the minimum dominating set problem (Sec. B 1); the domatic number problem (Sec. B 2); and the induced path problem (Sec. B 3). In Sec. V we place these results in a broader context.

II. BACKGROUND

A. Ammann Beenker Tilings

The quasicrystal structures represented by the Ammann-Beenker tilings lack the translation symmetry of periodic graphs and accordingly, mathematical results in the thermodynamic limit are more challenging to obtain. However, the translation symmetry of ordinary crystals is replaced by a *discrete scale symmetry* which underlies the unique features of quasicrystal systems. This symmetry is the reason why quasicrystals, like periodic crystals, display forms of long range atomic order, not present in purely random graphs.

We will first describe the construction of the AB tilings in the thermodynamic limit [42], and then discuss the scale symmetry of the tilings, which is central to our proof of Hamiltonian cycles.

Each tiling is built from two basic building blocks, called ‘prototiles’: a square tile and a rhombic tile with acute angle $\pi/4$. Both tiles are taken to have unit edge length. Starting from any ‘legal’ patch of a few tiles¹, the tiling is then built by repeatedly applying an ‘inflation rule’ to the tiles: every tile is first ‘decomposed’ into smaller copies of the two tiles, as defined in Fig. 2, and then the new edges are rescaled (inflated) by a factor of the silver ratio, $\delta_S = 1 + \sqrt{2}$, so that the tiles have unit edge length again. The edges and vertices of the tiling define a graph. The graph is bipartite, meaning the vertices divide into two subsets where edges of the graph only join members of one subset to the other. Since the arguments presented in this paper only rely on the connectivity of the graph, the rescaling is not important for our purposes — hence inflation and decomposition are interchangeable in what follows. Under inflation, the number of tiles grows exponentially and the infinite tiling is recovered in the limit

$$\mathcal{T} = \lim_{n \rightarrow \infty} \sigma^n(\mathcal{T}_0), \quad (1)$$

where \mathcal{T} is the infinite tiling, σ the inflation rule, and \mathcal{T}_0 the initial patch. We use “tiling” to mean the infinite tiling, and “patch” when referring to any finite set of connected tiles. The inverse process, termed ‘deflation’, equivalently ‘composition’ (followed by a rescaling), is uniquely defined and follows from the inflation rules.

The set of Ammann-Beenker tilings that can be created this way has infinite cardinality, and all tilings satisfy a strong property known as *local isomorphism*: any finite patch of tiles found in one tiling can be found, and recurs with positive frequency, within the given tiling and all

¹ Legal patches can be defined according to edge matching rules [42], and simply ensure that the starting patch corresponds to a group of tiles that can be found together within the infinite tiling. In practice, usually a single square or rhombus tile is used as the initial patch.

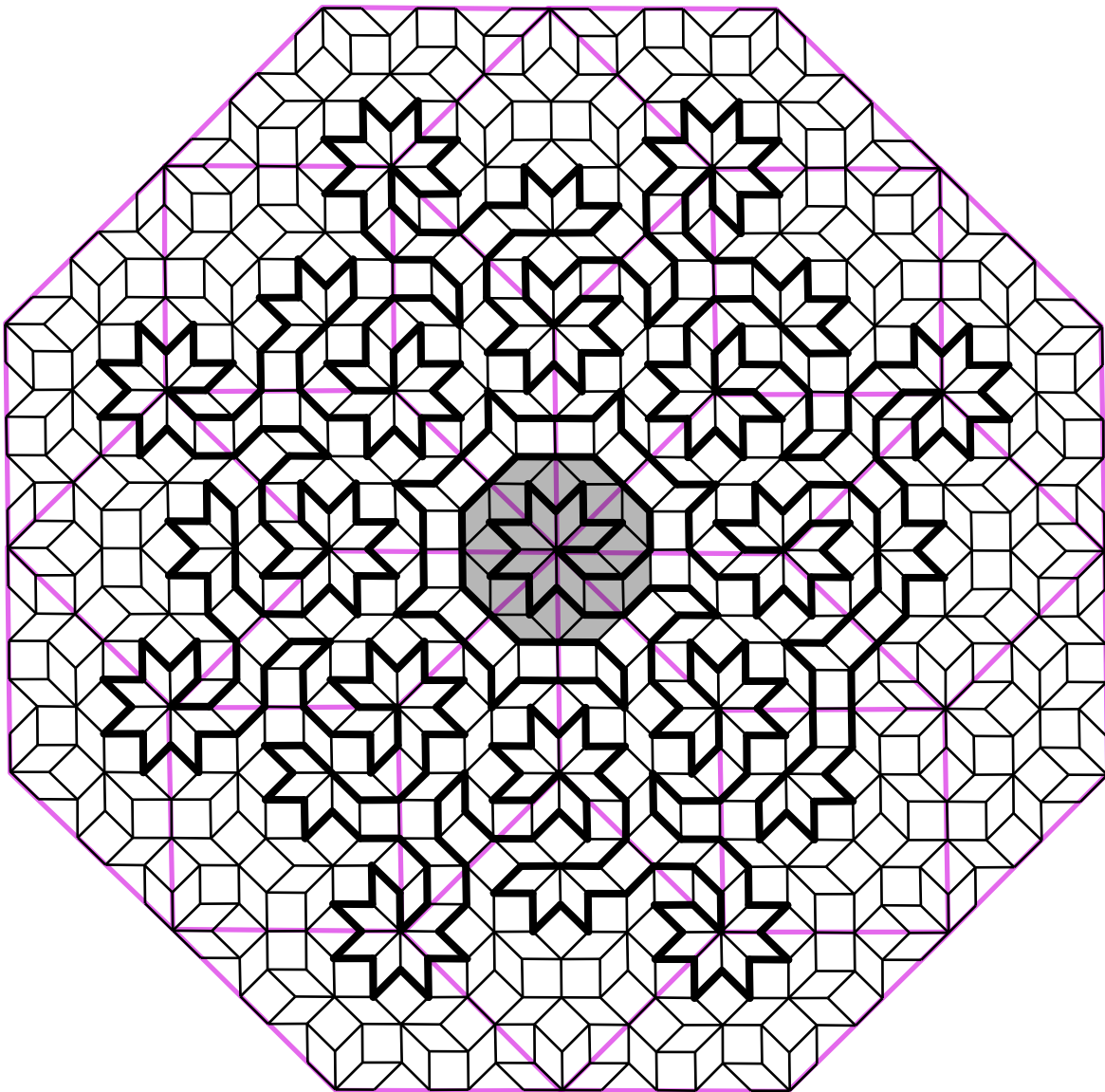


FIG. 1: A patch of AB tiling showing the 8-fold symmetric region W_1 , and W_0 in grey. W_1 is the twice-inflation of W_0 , formed from the double-inflated tiles shown in Fig. 2; purple lines show the boundary of these tiles (and do not belong to the tiling itself). The thick black edges form a Hamiltonian cycle on the set of vertices they visit; this set is termed U_1 .

other AB tilings [40, 42]. Within the locally isomorphic set we will not differentiate between arbitrary rescalings of the tilings. As the simplest example of this isomorphism, the set of edges and tiles surrounding each vertex in the tiling belongs to one of seven unique configurations, which we call ‘ m -vertices’ (where m labels the vertex connectivity). In total the vertex configurations for AB are given by the 3-, 4-, 5_A -, 5_B -, 6-, 7- and 8-vertices, with each configuration appearing with a frequency given by a function of the silver ratio δ_S . The 3-vertex, for example, occurs most frequently and makes up a fraction $\delta_S - 2$ ($\sim 40\%$) of the AB vertices. The two configura-

tions with five edges are distinguished by their behaviour under inflation.

A special role is played by the 8-vertices of the tiling, as every vertex configuration inflates to an 8-vertex under at most two inflations [39]. This means simply that if one was to ‘draw edges’ between the 8-vertices of an AB tiling, another AB tiling is generated. We refer to Fig. 1 where this symmetry is highlighted. Similarly, some of the 8-vertices of the original tiling sit also at 8-vertices of the composed tiling, and therefore logically form the *four-times* composed tiling. This hierarchy continues and results in the discrete scale symmetry exhibited by the

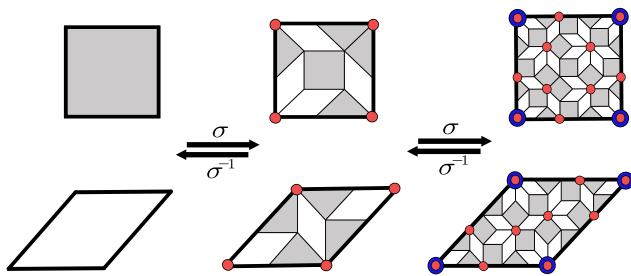


FIG. 2: The ‘inflation’ rule σ , in which a tile is decomposed into smaller tiles. Typically this would be followed by a rescaling (inflation) of all lengths by a factor of the silver ratio $\delta_S = 1 + \sqrt{2}$, although as we are only concerned with graph connectivity, inflation and decomposition are equivalent. Vertices of once- and twice-inflated tiles are shown in red and blue respectively. We denote the once-inflated tiles to be level $L_{1/2}$ and the twice-inflated tiles to be level L_1 .

AB tiling and several other aperiodic tilings, in turn responsible for many of the remarkable physical properties of quasicrystals.

We call an 8-vertex an 8_0 -vertex if under twice-deflation it becomes any m -vertex with $m \neq 8$ (most 8-vertices of the AB tiling are of this type); similarly we call it an 8_1 -vertex if it becomes an 8_0 -vertex under twice-deflation. Generalising, an 8_n -vertex becomes an 8_0 -vertex after $2n$ deflations. The *local empire* of a vertex is the simply connected set of tiles that always appears around the vertex wherever it appears in the tiling. The local empire of the 8_0 -vertex, which we call W_0 , is shown in Fig. 1 (also shown is the 8_1 empire, W_1): it has a discrete 8-fold rotational symmetry (D_8 in Schönflies notation). The inflation rule maps 8_n -vertices to 8_{n+1} -vertices (applying the rule twice) while simultaneously growing the size of the vertex’s local empire. The D_8 symmetry is preserved under inflation. Therefore 8_n -vertices are accompanied by D_8 -symmetric local empires W_n having a radius of symmetry growing approximately as $R_n \sim \delta_S^{2n}$. Due to the local isomorphism property, any finite patch of tiles can be found within the local empire of an 8_n -vertex for sufficiently large n : therefore we will often focus on these special cases to prove more general results. Furthermore the W_n empire contains all $W_{0 \leq m \leq n}$ empires. We also note that it is useful to define a modified version of the AB tiling with all 8-vertices removed, dubbed the AB* tiling [39].

In Fig. 2 we denote the individual square and rhombus (left) to be level L_0 and the *twice* inflated square and rhombus (right) to be level L_1 ; this is because any vertex inflates to an 8-vertex under two inflations but not one, and the convention follows Ref. 39. We therefore designate the *once*-inflated tiles (middle) to be at level $L_{1/2}$.

B. Graph terminology and conventions

A graph $G(V, E)$ is a set of vertices V connected by a set of edges E . We consider undirected graphs, in which no distinction is drawn between the two directions of traversal of an edge. We also consider only bipartite graphs, in which the vertices divide into two sets such that edges only connect one set to the other. The cardinality of a graph is the cardinality of the set of vertices it contains (i.e. the number of vertices in the graph). We denote this $|G|$ [77–79].

A ‘path’ is a set of edges joining a sequence of distinct vertices. Given a set of edges $E' \subset G$ it may be possible to find an ‘alternating path’, which is a path in G along which every second edge belongs to E' but all others do not [77]. We borrow this terminology from the theory of dimer matchings, in which E' is a set of edges such that no two edges share a common vertex, although we consider different structures for E' here. An ‘augmenting path’ is an alternating path in which the first and last edges are not in E' . In general, ‘augmenting’ an alternating path means to switch which edges along the path are in the set E' and which are not.

In this paper, we consider graphs made from the vertices and edges of Ammann-Beenker tilings. We will use the shorthand $G = \text{AB}$ to denote the case that G is the graph formed from any infinite Ammann-Beenker tiling. We will sometimes refer to graphs formed from finite patches of AB, which should be clear from context.

III. CONSTRUCTIVE PROOF OF HAMILTONIAN CYCLES

In this Section we prove the following theorem.

Theorem 1. *Given an AB tiling and a set of vertices $V \subset \text{AB}$ there exists a set U_n , where $V \subseteq U_n \subset \text{AB}$, such that U_n contains a Hamiltonian cycle \mathcal{H} .*

Proof. In Section III A we identify a set of edges on the twice-inflated AB tiles such that every $8_{n < 0}$ vertex (that is, every vertex which is not an 8-vertex) meets two such edges. This constitutes a set of fully packed loops (FPLs), visiting every vertex precisely once, on AB*. We then focus on finite tile sets generated by n twice-inflations of the local empire of the 8_0 -vertex, denoted W_n . These regions have D_8 symmetry. Any set of vertices $V \subset \text{AB}$ lies within an infinite hierarchy of W_n for sufficiently large n . In Section III B we identify a method of reconnecting these fully packed loops so as to include into the loops all 8_0 -vertices within W_n , and then all $8_{0 < m < n}$ vertices where the 8_{m-1} vertices have already been included. The result is fully packed loops on all vertices within W_n except the central 8_n vertex. Finally, we show that a subset of these loops can be joined into a single loop which additionally visits the central vertex. We denote the set of vertices visited by this loop U_n . This being a cycle which

visits each of its vertices precisely once, and which contains every vertex in V , we have proven Theorem 1. \square

The proof is constructive, returning \mathcal{H} given V , and is linear in the number of vertices in U_n . Furthermore, the Hamiltonian cycle on U_n visits a simply-connected set of vertices whose cardinality increases exponentially with n , and which therefore admits a straightforward approach to the thermodynamic limit. In this sense we can say that infinite AB tilings admit Hamiltonian cycles.

A. Constructing Fully Packed Loops on AB*

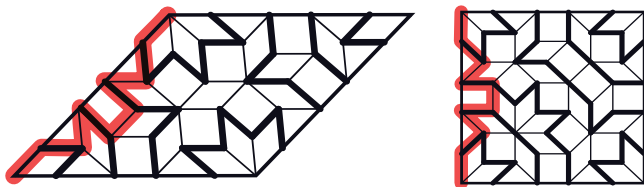


FIG. 3: Twice-inflations of each of the two AB prototiles. We denote the smaller tiles composition-level zero, L_0 , and the larger tiles L_1 . The thick black edges visit all but the corner vertices. We call these edges e_0 edges. Since the 8-vertices at L_0 corresponds to the tile vertices at L_1 , the union of e_0 constitutes fully packed loops on AB* (AB without the 8-vertices). Augmenting the red path (switching covered and non-covered edges) places loop ends on the two corner vertices while still visiting the original vertices. The red path can be thought of as the twice-inflation of an L_1 edge, and we term it e_1 . It has the same effect along any tile edge. Augmenting cycles built from e_1 then places all visited 8-vertices onto the same loop.

In Fig. 3 we show the twice-inflations of the two prototiles. We denote the smaller tiles as constituting composition level zero, L_0 , and the larger tiles L_1 . We work exclusively with twice-inflations, rather than single inflations, as every vertex becomes an 8-vertex under twice-inflation, but some do not do so under a single inflation.

In Fig. 3 we highlight (thick black edges) a set of edges on each L_1 tile. When the L_1 tiles join into legitimate AB patches, every vertex in L_0 is visited by precisely two thick edges except those vertices sitting at the corners of the L_1 tiles (and vertices on the patch boundary, which are not important when we take the thermodynamic limit). We call each of these edges an e_0 edge. The corner vertices of L_1 tiles are exactly the 8-vertices of L_0 (this follows from the fact that every vertex becomes an 8-vertex under at most two inflations). Therefore this choice causes every vertex of AB* at L_0 to be met by two e_0 edges. Since every vertex meets precisely two edges, the sets of edges must either form closed loops, or extend to infinity. In fact at most two can extend to

infinity [80]. Therefore these loops constitute a set of fully packed loops (FPLs) on AB* as required.

While it is possible to find other sets of edges with these properties, we designate this choice the canonical one. With it, all closed loops respect the D_8 local symmetry of AB and AB*.

B. Constructing Fully Packed Loops on AB

We next seek to construct FPLs on AB rather than AB* by adding the missing 8-vertices onto the loops. In Fig. 3 we highlight in red an alternating path (with respect to e_0 edges) which connects nearest-neighbour vertices in L_1 . Augmenting this path has a number of effects. First, it places string ends at the two L_0 8-vertices on which it terminates. Second, it increases the total number of e_0 edges by one. Third, any vertex which was previously visited by a pair of e_0 edges is still visited by a pair of e_0 edges.

While other such paths are possible, this canonical choice has advantages when combined with the canonical choice of e_0 edges. First, it can be seen in Fig. 3 that exactly the same shape of path can be used on any edge of either L_1 tile to cause the set of three effects just listed. Second, it does so entirely within the tile itself, and so these augmentations can be carried out without reference to neighbouring L_1 tiles. The augmentation can be undone by augmenting along the same path a second time, which turns out to be key.

The red alternating paths trace a route along L_0 graph edges which follows the L_1 edges as closely as possible while also alternating with reference to the e_0 edge placement. In a natural sense, then, the red path is the twice-inflation of an edge of an L_1 tile. We therefore refer to the red path as an e_1 edge. In this way, e_0 edges connect $8_{n<0}$ -vertices (i.e. any vertices *except* 8-vertices at L_0), while e_1 edges connect 8₀-vertices (8-vertices which can survive precisely zero deflations while remaining 8-vertices). Further inflations can be carried out by stitching e_1 edges together in exactly the same way that e_1 was formed from e_0 . For example, e_2 edges, connecting 8₁-vertices, can be built from e_1 edges, and can equivalently be thought of as built from more e_0 edges. In general, 8_n -vertices can be connected by e_{n+1} edges. Once again, these will naturally form D_8 -symmetrical loops in AB. The first three levels are shown in Fig. 4.

In the limit $n \rightarrow \infty$, e_n is a fractal: under $e_0 \rightarrow e_1$ the initial side length of any prototile is divided into 9 segments each of length δ_S^{-2} . The same scaling occurs for all subsequent inflations, and so the box counting dimension of e_∞ is given as

$$\dim(e_\infty) = \lim_{n \rightarrow \infty} \frac{\log(9^n)}{\log(\delta_S^{2n})} = \frac{1}{\log_3(1 + \sqrt{2})} \approx 1.246. \quad (2)$$

This fits with the intuition that the curve is space-filling.

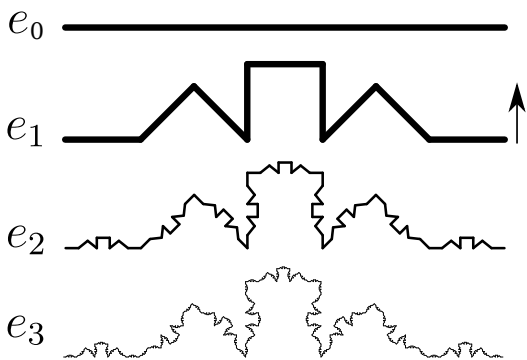


FIG. 4: The red alternating path in Fig. 3 can be thought of as a twice-inflation of an e_0 edge from which loops are constructed at level zero (L_0). It connects nearest neighbours in the L_1 tiling (8-vertices in the L_0 tiling) while following an alternating path in the canonical choice of e_0 placements. We therefore denote this path an e_1 edge. Alternating paths connecting higher-order 8_n -vertices can be constructed by concatenating e_{n+1} edges in the same way that e_1 was formed from a concatenation of e_0 ; levels e_2 and e_3 are shown here. We define the orientation of e_n according to the arrow.

To complete the proof of the existence of an FPL on AB it remains to show that all 8-vertices can be placed onto closed e_n -loops for sufficiently large n . The canonical edge covering places all $8_{n < 0}$ vertices of AB onto e_0 -loops. To add all 8_0 -vertices onto loops, we place loops of e_1 edges according to the canonical edge placement. This placement was defined at level L_0 ; but note that the twice-(de)composition of any AB tiling is another AB tiling. Therefore the placement is well defined at all levels. Placing an e_1 edge means augmenting a path at L_0 . Augmenting the closed loops of paths just defined places all 8_0 -vertices visited by that loop onto loops of e_0 edges as required. We then proceed by induction, adding 8_n -vertices by connecting them with loops of e_{n+1} edges. After n steps, every vertex of order $8_{\leq n}$ is contained in a set of fully packed loops defined on those vertices. By design, placing the e_n edges does not cause problems with the existing matching of e_{n-1} edges.

While e_1 edges must follow the edges of L_1 tiles, two tiles meet along any edge. There is therefore a choice of two orientations of each e_1 owing to the choice of which of the two tiles e_1 lies within. Each e_1 orientation can be chosen freely with the statements in the previous paragraph remaining true. However, we find that there is again a natural choice. Define the orientation of e_1 to be in the direction indicated in Fig. 4. At L_1 , we choose the sequence of e_1 edges along a loop to point alternately into then out of the loop on which it sits (this is implicit in the construction of e_2 and e_3 in Fig. 4). Since AB is bipartite, all loops are of even length, and there is never an inconsistency. When e_2 edges are placed, these will

cut through e_1 -loops. It is always possible to choose the orientations so that wherever e_1 -loops and e_2 -loops intersect, they do so along the length of one e_1 (recall that an e_2 is built from multiple e_1). Since these two e_1 overlap perfectly, augmenting them both has no overall effect at L_0 . We can therefore delete both e_1 . The effect is that the L_2 loops no longer intersect the L_1 loops: instead, they rewire separate L_1 loops so as to make them join together. By induction the rewiring works at all levels. The process is shown in detail in Appendix A, Fig. A.1 and Fig. A.2.

Loops constructed to level n visit all vertices within a region of D_8 -symmetry centred on an 8_n -vertex, with the sole exception of the vertex itself. While it is already possible to reconnect many of these loops together, thereby building Hamiltonian cycles on subsets of the W_n vertices, the sets of vertices visited by such cycles always encircle sets of vertices they do not visit. This is displeasing, since in the limit of an infinite number of inflations only a finite percentage of vertices of AB would then be visited by the largest Hamiltonian cycle. To remedy this, it is necessary to break the D_8 symmetry. To see that this is necessary, consider the simplest D_8 Hamiltonian cycle, which is a star visiting the eight vertices adjacent to any 8-vertex, and the eight vertices immediately beyond them. To include the central 8-vertex on a loop, one of the points of the star must turn inwards, breaking the symmetry.

In Fig. 5 we show a simple way to include the central region. The outermost e_n -loop encircling the 8_n -vertex is the $2n$ -fold inflation of the smallest star loop. By folding in a single corner of this inflated star, the loop now visits the central 8_n -vertex. In so doing, it connects *every* loop contained within it (and all those it passes through) into a single loop. The result is therefore a Hamiltonian cycle on the simply-connected set of vertices visited by this deformed star. We denote this set U_n to distinguish it from the D_8 symmetric set W_n .

In general we can say that for any disk of radius R there exists a set of vertices U_n which encompasses the disk, on which we can construct a Hamiltonian cycle by the method just outlined. The algorithm is of linear complexity in the number of vertices within U_n . The cycle U_2 is shown in Fig. 6. We can take the limit $R \rightarrow \infty$ without issue; the set U_∞ defines one possible thermodynamic limit of AB in which every vertex is visited by the same Hamiltonian cycle. In this sense we can say that AB tilings admit Hamiltonian cycles.

It should be noted that an AB tiling can have at most one global centre of D_8 symmetry (more than one would violate the crystallographic restriction theorem [81]), and the set of tilings with a global D_8 centre is measure zero in the set of all possible AB tilings [42]. However, our definition of the thermodynamic limit does not rely on our tiling having a global D_8 centre – it only needs to contain at least one U_∞ , and all AB tilings contain infinitely many. Our thermodynamic limit contains infinitely many vertices, but in the present construction

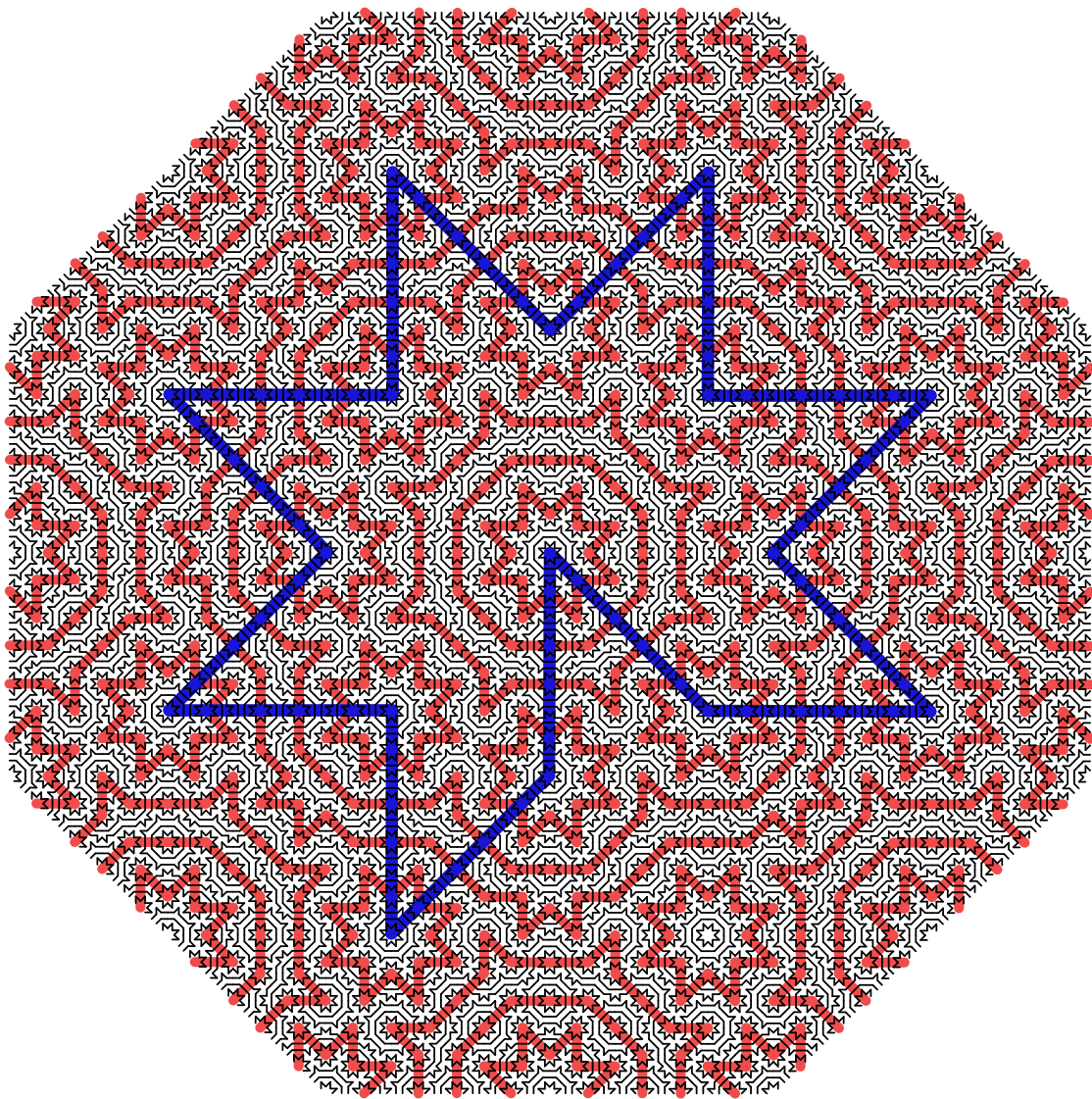


FIG. 5: The canonical placements of e_0 edges (black) form e_0 -loops visiting every $8_{n<0}$ -vertex (i.e. every vertex which is not an 8-vertex). The red lines form e_1 -loops, along which e_1 edges from Fig. 4 can be placed adding all 8_0 -vertices onto loops. Similarly the blue star forms a e_2 -loop, along which e_2 edges from Fig. 4 can be placed adding 8_1 -vertices onto loops (see Fig. A.1). The central 8-vertex is now added onto loops by folding one corner of the blue star inwards to break the 8-fold symmetry. Here we have shown the process explained in Sec. III B to order $n = 2$, but it can be iterated to any order n .

it only contains *all* vertices in the special case that the tiling is U_∞ . Hamiltonian cycles on other sets of vertices can be constructed by choosing different routes for the largest loop (alternatives to the star with a folded-in corner).

IV. SOLUTIONS TO OTHER NON-TRIVIAL PROBLEMS ON AB

The question of whether an arbitrary graph admits a Hamiltonian cycle lies in the complexity class NPC.

Problems in NPC are decision problems, meaning they are answered either by yes or no. The optimisation version of these problems – to provide a solution if one exists – is instead typically in the class NP-Hard (NPH). Finding a Hamiltonian cycle on an arbitrary graph is NPH.

In this section we provide exact solutions on AB for three problems made tractable due to discrete scale symmetry and/or by our construction of Hamiltonian cycles. In each case we state the decision problem and the corresponding optimisation problem. Our choice of problems is motivated by the fact that on general graphs these decision problems lie in the complexity class NPC, and the

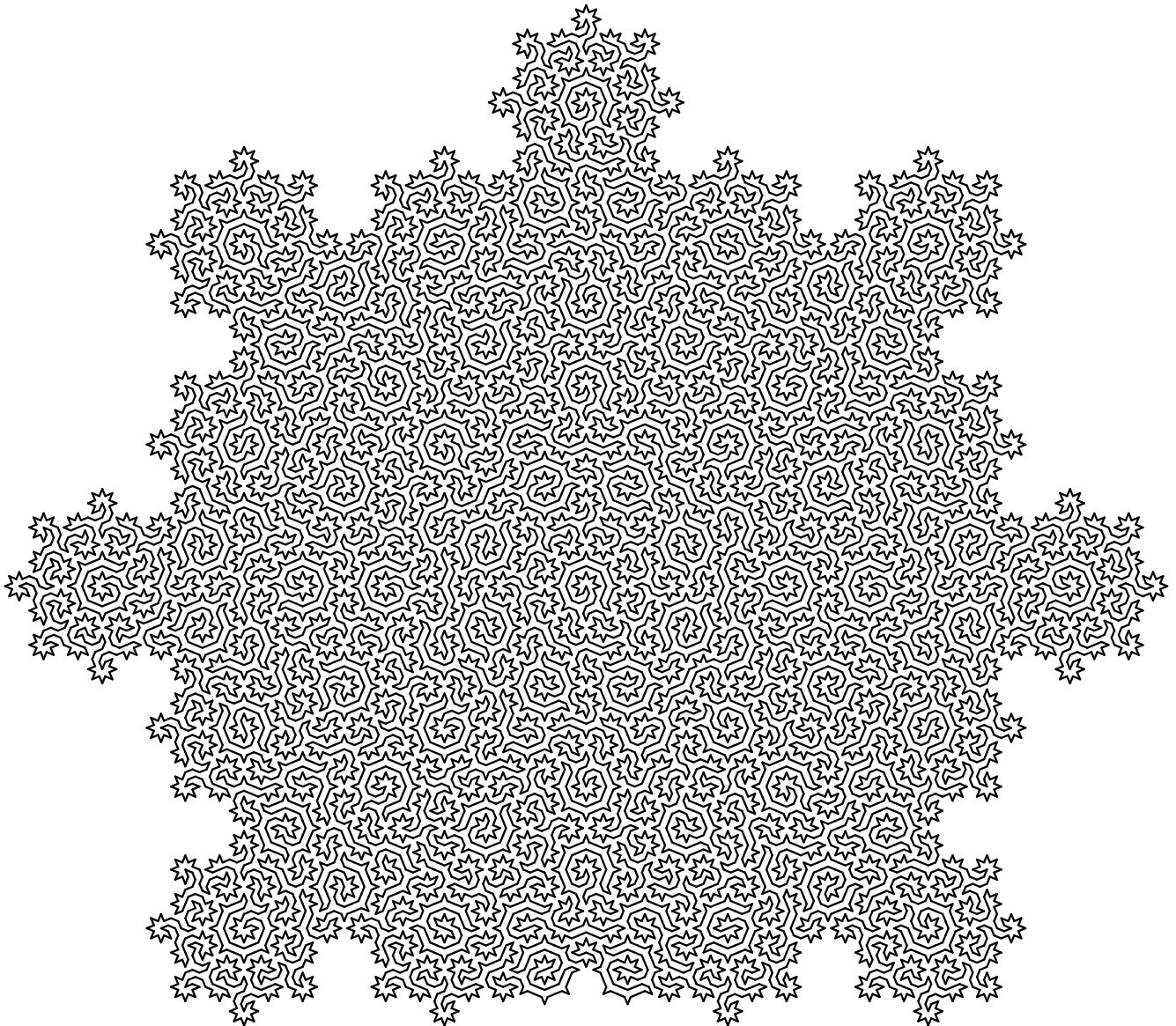


FIG. 6: The Hamiltonian cycle visiting all the vertices of a U_2 region (the AB tiles themselves are omitted for clarity). The image is obtained from Fig. 5 by placing e_1 and e_2 edges in alternate orientations along the red and blue loops respectively, as shown in Fig. A.1, and augmenting. Note the present figure has been rotated through $1/16^{\text{th}}$ of a turn relative to other figures to utilise the page efficiently.

corresponding optimisation problems lie in the complexity class NPH. By solving the problems on AB we again show that this setting provides a special, simpler case.

A. The Equal-Weight Travelling Salesperson Problem

Problem statement [63, 82]: given a number of cities N , unit distances between each pair of connected cities, and an integer k , does there exist a route shorter than k which visits every city exactly once and returns

back to the original city? The corresponding optimisation problem is to find such a route.

Solution on AB: if cities are the vertices of $U_{n \geq 0}$, yes iff $k > |U_n|$.

Proof: from a graph theory perspective, we can consider every city as a vertex and every direct route between a pair of cities as a weighted edge, where the associated weight denotes the distance between those cities. Finding the shortest route which can be taken by the travelling salesperson is equivalent to finding the lowest-weight Hamiltonian cycle, where the weight of the cycle is the sum of the weights of its edges.

In this paper we have considered the unweighted AB graph, equivalent to setting all edge weights to one. In unweighted graphs the problem reduces to the equal-weight travelling salesperson problem. After this simplification, the unweighted decision problem becomes equivalent to the Hamiltonian cycle problem. Therefore the Hamiltonian cycle constructed in Section III solves the equal-weight travelling salesperson optimisation problem on U_n .

Application: scanning microscopy

One physical application of the travelling salesperson problem is to find the most efficient route to scan an atomically sized tip across a surface so as to visit every atom. For example, scanning tunneling microscopy (STM) involves applying a voltage between an atomically sharp tip and the surface of a material. Electrons tunnel across the gap between the tip and the sample, giving a current proportional to the local density of states in the material under the tip [83, 84]. Magnetic force microscopy (MFM) uses a magnetic tip to detect the change in the magnetic field gradient [85, 86]. The ultra-high resolution nature of the imaging means that state of the art measurements might take on the order of a month to scan a $100\text{ nm} \times 100\text{ nm}$ square region of a surface². While generally applied to periodic crystalline surfaces, STM and MFM can in principle be used to image the surfaces of aperiodic quasicrystals, including those with the symmetries of AB tilings [45]. Unlike in the crystalline case, the most efficient route for the STM tip to visit each atom is not obvious in these cases. Our solution to the TSP optimisation problem on AB provides a maximally efficient route for aperiodic quasicrystals with the symmetries of AB tilings. While the surface would need to be scanned once in order to establish the U_n regions to study, the purpose of STM and MFM would be to detect changes in the material under changing conditions (say, temperature or magnetic field), and the route provides maximum efficiency upon multiple scans.

B. The Longest Path Problem

A *simple path* is a sequence of edges in a graph which lacks repeating vertices.

Problem statement [63, 87]: given an unweighted graph G and an integer k , does G contain a simple path

of length at least k ? The corresponding optimisation problem is to find a maximum length simple path.

Solution: yes, if $G = \text{AB}$.

Proof: a Hamiltonian path is a simple path. The results of Section IV A imply that there exists a simple path of length $|U_n| - 1$ in any region U_n . Since any (infinite) AB tiling contains regions U_∞ , it follows that any AB tiling contains simple paths of any length (finite or infinite).

Comment: deleting any single edge from the Hamiltonian cycle constructed in Sec. III produces a Hamiltonian path connecting its two end vertices. This path is of length $|U_n| - 1$, the longest possible k . A path for any shorter k can be found simply by deleting further contiguous edges. Our construction provides a solution for the longest path optimisation problem on AB as it gives the maximum length simple path on the tiling after removing any single edge on the cycle.

Application: adsorption

The ‘dimer model’ in statistical physics seeks sets of edges on a graph such that each vertex connects to precisely one edge. It was originally motivated by understanding the statistics and densities of efficient packings of short linear molecules adsorbed onto the surfaces of crystals [88–90]. Noting again that certain physical quasicrystals have the symmetries of AB tilings on the atomic scale, the existence of a longest path visiting every vertex shows that a long flexible molecule such as a polymer could wind so as to perfectly pack an appropriately chosen surface of such a material. The path can be broken into segments of any smaller length, showing that flexible molecules of arbitrary length can pack perfectly on to the surface. Dimers are returned as a special case.

Adsorption has major industrial applications. In catalysis, for example, reacting molecules can find a reaction pathway with a lower activation energy by first adsorbing onto a surface. While efficient packings can be identified on periodic crystals such as the square lattice, these feature a limited range of nearest-neighbour bond angles (with only right angles appearing in the square lattice). Realistic molecules, which have some degree of flexibility, might do better on quasicrystalline surfaces which necessarily contain a range of bond angles (four in AB). Other uses could include (hydro)carbon sequestration and storage, and protein adsorption [88, 90].

C. The Three-Colouring Problem

Problem statement [63, 91]: can all the faces of a planar graph G be coloured such that no faces sharing an edge share a colour? The corresponding optimisation problem is to find such a three-colouring.

Solution: yes, if $G = \text{AB}$.

² State of the art STM measurements can obtain intra-unit-cell data on crystal surfaces; for a 100×100 sq-nm region this would exceed 250,000 pixels. A typical measurement takes around 100 ms, so if each pixel is scanned at 100 energies, the result takes around 29 days. We thank J. C. S. Davis for these estimates.

Proof: we know that the AB tiling is a bipartite graph which means that its vertices can be partitioned into two disjoint sets such that none of the edges has vertices belonging to the same set. We associate two opposite bipartite ‘charges’ to the vertices depending upon which of these two mutually exclusive sets they belong to.

We define two three-coloured tiles, 1 and 2, as shown in Figs. 7(a) and (b), and repeat them over the entire tiling in the following manner.

- Place tile 1 over any 8-vertices having the same bipartite charge.
- Place the mirror image of tile 1 over any 8-vertices having the opposite bipartite charge.
- After that, place tile 2 or its mirror image such that the three rhombuses around every ladder, shown in Fig. 7(c), are the same colour.

The consistent placement of these two tiles on the whole tiling is ensured by the structure of the tiling itself. After filling the whole AB tiling with these two tiles all that remain are ladders, as shown in Fig. 8, which can be coloured consistently on the basis of colors of their surrounding rhombuses such that no two adjacent faces should have a same colour.

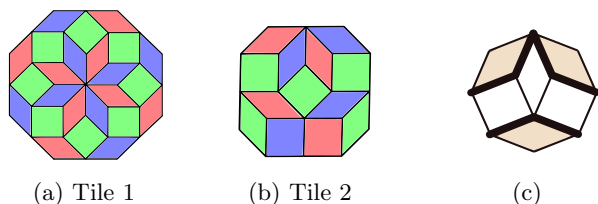


FIG. 7: (a),(b) Tiles used for 3-colouring of the AB tiling. (c) The structure with three rhombuses present around every ladder.

The 3-colouring solution for the AB tiling is shown in Fig. A.3. Note that the three-colourings are not unique.

Comments: the five-colouring theorem, which states that any political map requires at most five colours in order to avoid any neighbouring countries being the same colour, was proven in the 19th century [92]. The equivalent four-colouring theorem was an infamous case of a problem which is easy to state but difficult to solve. The eventual proof in 1976 was the first major use of theorem-proving software, and no simple proof has been forthcoming [93]. The three-colouring problem is known to be NPC [63] on general graphs. However, special cases can again be solved. A polynomial-time algorithm for generating a three-colouring of the rhombic Penrose tiling was deduced in 2000, following its conjectured existence by Conway[94]. The proof in fact covers all tilings of the plane by rhombuses, and therefore includes AB tilings. Our own solution to the three-colouring problem on AB tilings takes a different approach, and generates different three-colourings.

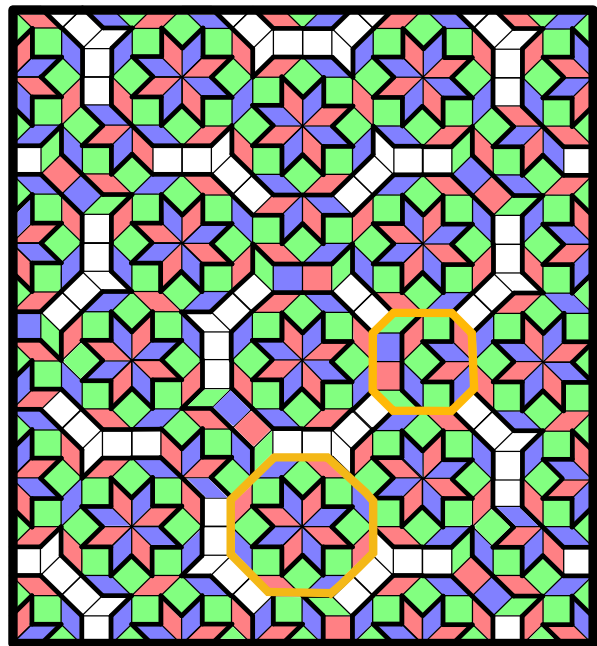


FIG. 8: A small patch of AB tiling 3-coloured using tile 1 and tile 2 (both outlined in gold) as mentioned in Sec IV C. The only remaining portions of the tiling are segments of ladders which can be 3-coloured consistently on the basis of their surrounding tiles.

1. Application: the Potts model and Protein folding

The q -state Potts model, $q \in \mathbb{N}$, is a generalisation of the Ising model to spins σ_i which can take one of q values [69]. It is defined by the Hamiltonian

$$H = -J \sum_{\langle ij \rangle} \delta_{\sigma_i, \sigma_j} \quad (3)$$

where the sum is over nearest neighbours and δ is the Kronecker delta [69]. We can define the Potts model on the AB tiling by placing one spin on the centre of each face of the tiling, with the four nearest neighbours defined to be the spins situated on the faces reached by crossing one edge.

The Potts model has a broad range of applications in statistical physics and beyond. It shows first and second order phase transitions, and infinite order BKT transitions, under different conditions of J and q . It is used to study the random cluster model [95], percolation problems [96] and the Tutte and chromatic polynomials [97]. Its physical applications include quark confinement [98], interfaces, grain growth, and foams [96], and morphogenesis in biological systems [99]. While most extensively studied on periodic lattices, there is some work on the Potts model in Penrose tilings; this model appears to show the universal behaviour present in the periodic cases [100, 101].

For $J > 0$ the model has a ferromagnetic ground state with all spins aligned along one of their q directions.

The behaviour for $J < 0$ is more complex. For $q = 2$ the model is the Ising model; since a two-colouring of the faces of AB is impossible (ruled out by the existence of 3-vertices), the antiferromagnetic ground state must be geometrically frustrated, meaning the connectivity of sites causes spins to be unable to simultaneously minimise their energies.

However, the existence of a face-three-colouring proves that for $q \geq 3$ the $J < 0$ state is again unfrustrated. Three-colourings give the possible ground states of $q = 3$, and a subset of ground states for $q \geq 4$.

The relationship between the Potts model and the process of protein folding has been widely studied in the field of polymer physics and computational biology [75, 76, 102]. The q -state Potts model has been used to model the thermodynamics of protein folding [103]. In this scenario the lattice is thought of as a solvent in which the protein exists. A protein is a chain of amino acids [13]. When dissolved it may achieve a stable configuration, typically remarkably compact, which enables its biological functions [14]. The folding process depends on the pair-wise interactions between amino acids, set by the interaction with the solvent [1, 13, 75]. If the interactions between similar amino acids are attractive, they cluster together to form a compact folded structure. If these interactions are repulsive, similar amino acids try to spread out over the solvent sites, resulting in a protein which is folded, but not compactly [76]. For modelling proteins, the Hamiltonian in Eq. (3) represents interacting amino acids $\{\sigma_i\}$. For $J < 0$ similar amino acids will have repulsive interactions in a solvent according to Eq. (3). For $J < 0$ and protein chains consisting of only three different types of amino-acids (each corresponding to a colour), our three-colouring of AB also predicts one of the stable, minimum energy configurations in which the protein can fold such that each of the three types of amino acid sits on the centre of a tile of corresponding color.

It seems reasonable to suppose that folding of long protein chains might be better modelled by approximating the solvent with a quasicrystalline surface rather than a simple periodic lattice. This is because quasicrystals provide an aperiodic surface with range of bond angles, unlike regular lattices which have restricted freedom. For instance, square and hexagonal lattices have only one bond angle each (90° and 120° respectively), and one vertex type, whereas AB has three bond angles of 45° , 90° , and 135° , and a wide range of different local environments branching out from seven vertex types. The 8-fold rotational symmetry of patches of AB is of a higher degree than is possible in any crystal (six being the maximum degree permitted by crystallographic restriction), additionally making AB a closer approximation to the continuous rotational symmetry of space.

V. CONCLUSIONS

We provided exact solutions to a range of problems on aperiodic long-range ordered Ammann-Beenker (AB) tilings, with a further three problems solved in Appendix B. There are undoubtedly many more non-trivial problems like these which can be solved on AB tilings by taking advantage of its discrete scale invariance.

To our knowledge only one of the problems we solved was covered by an existing result: the three-colour problem was covered by a solution to the three-colour problem for Penrose tilings which applied to all tilings of rhombuses [94]. It is reasonable to ask whether this previously known result might similarly have been used to solve a range of other problems on AB, in the same way we exploited solutions to the Hamiltonian cycle problem. While we cannot rule this out, three-colourings do not obviously seem to provide an organising principle for the tiling in the way that our hierarchically constructed loops do.

Our construction relies on the fact that AB tilings are long-range ordered, allowing exact results to be proven in contrast to random structures. It is natural to wonder whether any of our results apply more generally in other quasicrystals. Deleting every second edge along a Hamiltonian cycle creates a perfect dimer matching (division of the vertices into unique neighboring pairs). The existence of such a matching on a graph is therefore a necessary condition for the existence of Hamiltonian cycles. It is not a sufficient condition, as there exist efficient methods, such as the polynomial-time Hopcroft Karp algorithm, for finding perfect matchings [104]. Seeking quasicrystals which admit perfect matchings might be a good starting point for finding other quasicrystals which admit Hamiltonian cycles. As a preliminary check, using the Hopcroft Karp algorithm we found the minimum densities of unmatched vertices on large finite patches of quasiperiodic tilings generated using the de Bruijn grid method, with rotational symmetries from 7-fold up to 20-fold [105]. We found finite densities in each case, suggesting AB may be unique among the de Bruijn tilings in admitting perfect matchings or Hamiltonian cycles³. On the other hand, a preliminary check of the recently discovered ‘Hat’ [106] and ‘Spectre’ [107] aperiodic monotiles (single tiles which tile only aperiodically) suggest that these also admit perfect dimer matchings, even if vertices are added so as to make the graphs bipartite; however, the structure of these matchings seems to indicate that a continuation to fully packed loops is not possible.

Our Hamiltonian cycle construction included a proof of the existence of fully packed loops on AB, in which every vertex is visited by a loop, but these need no longer be the same loop [108]. The FPL model is important

³ We used Josh Colclough’s code for generating arbitrary de Bruijn grids, available at github.com/joshcol9232/tiling.

for understanding the ground states of frustrated magnetic materials such as the spin ices [7]. Famously, loops played a key role in Onsager’s exact solution to the Ising model in the square lattice, one of the most important results in statistical physics [109, 110]. If all loops could be enumerated systematically, this would suggest the Ising model with spins defined on the faces of AB might be exactly solvable. We note that all possible dimer matchings were exactly enumerated on a modification of AB in which all the 8-vertices were removed, giving the partition function to the dimer problem [39]. The possible loop configurations can similarly be enumerated in that context.

There is a deep connection between loop and dimer models, and quantum electronic tight-binding models defined on the same graphs. For example, Lieb’s theorem states that if a bipartite graph has an excess of vertices belonging to one bipartite sublattice, the corresponding tight-binding model must have at least the same number of localised electronic zero modes making up a zero-energy flat band [111]. These zero modes are topologically protected in the sense that they survive changes to the hopping strengths provided these strengths remain non-zero. Even if a bipartite graph has an overall balance of sublattice vertices, it can have locally defective regions in which zero modes are similarly localised [112]. This occurs for example in the rhombic P3 Penrose tiling, which has an overall balance between bipartite sublattices, but local imbalances lead to a finite density of localised electronic zero modes in its tight-binding and Hubbard models [113–115], which can be exactly calculated using dimers [61]. Even if the bipartite sublattices balance *locally*, as in the AB tiling [39], it could still in principle be the case that the graph connectivity localises electrons to certain regions. Recent work has identified such zero modes in the Hubbard model on AB [116]. Many, but not all, of these appear to fit a loop-based structure first identified in Penrose tilings [113] and subsequently more general graphs [117]. The same structures have recently been identified in the Hat aperiodic monotiles [118]. A deeper connection between the graph connectivities leading to electronic zero modes, and the loops we identify here, is an interesting avenue for further work.

Hamiltonian cycles and other loop models have been widely used for modelling protein folding, by approximating the molecules as living on the sites of a periodic lattice [1, 9, 76]. This simplification has allowed the tools of statistical physics to be brought to bear on complex problems [1, 15, 16]. Quasicrystals may well serve as better models for such studies in which space is approximated with a discrete structure. Quasicrystals are able to feature higher degrees of rotational symmetry than crystals, providing a better approximation to the continuous rotational symmetry of real space [44]. They feature a wider range of nearest neighbour bond angles, and the variety of structures at greater numbers of neighbours increases rapidly. Quasicrystals also lack discrete translational symmetry, a feature of lattices which could cause

them to poorly approximate continuous space, although quasicrystals such as AB do feature a discrete scale invariance which might lead to similar shortcomings. Random graphs also have these benefits, but they lack the long-range order of quasicrystals required to obtain exact results such as those we have presented here.

In the context of NPC problems, exact solutions to Hamiltonian cycles are useful because they serve as bench-marking measures for new algorithms [119–121]. While the difficulty of NPC means no known algorithm is capable of deterministically solving all instances in polynomial time, several algorithms display a high success rate on many graphs [119, 122, 123]. Finding and classifying Hamiltonian cycle instances which prove ‘hard’ for these algorithms has immediate practical applications and can provide key insight into the full NPC problem. A future goal would be to see how these modern Hamiltonian cycle algorithms perform when applied to AB regions admitting Hamiltonian cycles. Since AB sits at the borderline between regular and random graphs, it contains structures not present in either. Additionally, our Hamiltonian cycle construction is highly non-local, leveraging our understanding of the discrete scale symmetry of the tiling. Thus, it may prove a difficult test-case: in that scenario, understanding which structures of AB prove hard for solvers would be a worthwhile challenge. We provided our U_1 and U_2 graphs to the developers of the state-of-the-art ‘snakes and ladders heuristic’ (SLH) Hamiltonian cycle algorithm [119], who ran a preliminary test in this direction⁴. U_1 contains 464 vertices and U_2 contains 14992 vertices. The SLH algorithm found a Hamiltonian cycle on U_1 in modest time ($\sim 1s$) but failed to find cycles on U_2 before exceeding the allotted memory. Given the large size of U_2 however, this is not conclusive evidence that AB is hard to solve. A next step would be a more thorough analysis, possibly identifying Hamiltonian cycle regions of more reasonable size for bench-marking purposes.

Another interesting direction might be to consider directed or weighted extensions of the graphs. Directed graphs can model non-Hermitian systems with gain and loss [124]; weighted graphs could model, for example, the travelling salesperson problem in which cities are connected by different distances. Finding a shortest route through a weighted graph is still an NPC problem, and the route would be selected from among the unweighted Hamiltonian cycles.

Our solution to the longest path problem shows that sets of flexible molecules of arbitrary lengths (not necessarily the same) can pack perfectly onto AB quasicrystals if they register to the atomic positions. This suggests applications to adsorption, which is relevant for instance to

⁴ The SLH algorithm was run on an *Intel Core i7-1165G7* machine with 4 cores, 2.80 GHz clockspeed, and 32 GB RAM. We thank Michael Haythorpe [119] for running the SLH Hamiltonian cycle algorithm.

carbon capture [125] and catalysis: two molecules might find a lower-energy route to reacting if they first bond to an appropriate surface before being released after reaction. Physical quasicrystals with three-dimensional point groups – ‘icosahedral’ quasicrystals (iQCs) – are known to have properties which make them potentially advantageous as adsorbing substrates. Being brittle, they are readily broken into particles tens of nanometres in diameter, maximising their surface area to volume ratio (a key consideration in industrial catalysis). They are stable at high temperatures, facilitating increased rates of reactions [126]. And, as discussed above, their surface atoms, lacking periodic arrangements, permit a wider range of bond angles. On the other hand, iQCs have been found to have high surface reactivities, which is unfavourable for catalysis because adsorbing molecules will tend to bond to the iQC substrate rather than to one another [127, 128]. They also have low densities of states at the Fermi level compared to metals, which is unfavourable [53]. However, iQC nanoparticles have been successfully coated with atomic monolayers which then adopt their quasicrystallinity [129, 130]; these monolayers include silver, a widely used and efficient catalyst with none of the quasicrystals’ shortcomings [131]. Investigating the use of quasicrystals for such applications would therefore seem a profitable direction for future experiments.

The surfaces of iQCs have not been seen to feature the symmetries of AB; rather, they form a class of structures which includes Penrose tilings [127, 128]. Further work is therefore needed to establish the possible packing densities of realistic iQC surfaces. Alternatively, the

results presented here could potentially be put to use in the known two-dimensional ‘axial’ quasicrystals which feature the symmetries of AB [45, 46, 132].

While AB tilings might have appeared to be an unlikely place to seek exact results to seemingly intractable problems, owing to their lack of periodicity, their long-range order makes such results obtainable. While periodic lattices feature a discrete translational symmetry which simplifies many problems (essentially enabling fields such as condensed matter physics, floquet theory, and lattice QCD), quasicrystal lattices such as AB feature instead a discrete scale invariance. While less familiar, this is just as powerful a simplifying factor. Broadly, we might expect that many problems for which crystals are special cases might now find quasicrystals to also be special cases, albeit of a fundamentally different form.

ACKNOWLEDGMENTS

We thank J. C. Séamus Davis for providing estimates for scanning tunneling microscopy times, Francesco Zamponi for suggestions on Hamiltonian cycle benchmarking, Michael Haythorpe for running the SLH Hamiltonian cycle finder algorithm on AB regions, Michael Baake, Zohar Ringel, Steven H. Simon, Michael Sonner and Jasper van Wezel for helpful comments on the manuscript and Josh Colclough for the use of his code for generating de Bruijn grids.

-
- [1] H. S. Chan and K. A. Dill, Compact polymers, *Macromolecules* **22**, 4559 (1989).
 - [2] P.-J. Flory, Statistical thermodynamics of semi-flexible chain molecules, *Proceedings of the Royal Society of London. Series A. Mathematical and Physical Sciences* **234**, 60 (1956).
 - [3] H. Li, R. Helling, C. Tang, and N. Wingreen, Emergence of preferred structures in a simple model of protein folding, *Science* **273**, 666 (1996), <https://www.science.org/doi/pdf/10.1126/science.273.5275.666>
 - [4] H. E. Stanley, Dependence of critical properties on dimensionality of spins, *Physical Review Letters* **20**, 589 (1968).
 - [5] H. Blöte and B. Nienhuis, Fully packed loop model on the honeycomb lattice, *Physical review letters* **72**, 1372 (1994).
 - [6] R. J. Baxter, *Exactly Solved Models in Statistical Mechanics* (Academic Press, Harcourt Brace Jovanivich (London), 1982).
 - [7] L. Jaubert, M. Haque, and R. Moessner, Analysis of a fully packed loop model arising in a magnetic coulomb phase, *Physical review letters* **107**, 177202 (2011).
 - [8] J. Des Cloizeaux and G. Jannink, *Polymers in solution: their modelling and structure*, (No Title) (1990).
 - [9] O. Bodroza-Pantic, B. Pantic, I. Pantic, and M. Bodroza-Solarov, Enumeration of Hamiltonian cycles in some grid graphs, *MATCH Commun. Math. Comput. Chem* **70**, 181 (2013).
 - [10] G. Jannink, *Polymers in solution: Their modelling and structure* (Clarendon Press, 2010).
 - [11] B. Nienhuis, Exact critical point and critical exponents of O(n) models in two dimensions, *Physical Review Letters* **49**, 1062 (1982).
 - [12] J. L. Jacobsen and J. Kondev, Conformal field theory of the flory model of polymer melting, *Physical Review E* **69**, 066108 (2004).
 - [13] T. E. Creighton, Protein folding, *Biochemical journal* **270**, 1 (1990).
 - [14] K. A. Dill, S. Bromberg, K. Yue, H. S. Chan, K. M. Ftebig, D. P. Yee, and P. D. Thomas, *Protein science* **4**, 561.
 - [15] H. S. Chan and K. A. Dill, Intrachain loops in polymers: Effects of excluded volume, *The Journal of chemical physics* **90**, 492 (1989).
 - [16] K. F. Lau and K. A. Dill, A lattice statistical mechanics model of the conformational and sequence spaces of proteins, *Macromolecules* **22**, 3986 (1989).

- [17] J. L. Jacobsen, Exact enumeration of Hamiltonian circuits, walks and chains in two and three dimensions, *Journal of Physics A: Mathematical and Theoretical* **40**, 14667 (2007).
- [18] R. Agarwala, S. Batzoglou, V. Dančák, S. E. Decatur, M. Farach, S. Hannenhalli, S. Muthukrishnan, and S. Skiena, Local rules for protein folding on a triangular lattice and generalized hydrophobicity in the HP model, in *Proceedings of the first annual international conference on Computational molecular biology* (1997) pp. 1–2.
- [19] W. Orr, Statistical treatment of polymer solutions at infinite dilution, *Transactions of the Faraday Society* **43**, 12 (1947).
- [20] M. N. Barber and B. W. Ninham, *Random and restricted walks: Theory and applications*, Vol. 10 (CRC Press, 1970).
- [21] P.-G. De Gennes, *Scaling concepts in polymer physics* (Cornell university press, 1979).
- [22] K. F. Freed, Renormalization group theory of macromolecules, (No Title) (1987).
- [23] J. L. Jacobsen, On the universality of fully packed loop models, *Journal of Physics A: Mathematical and General* **32**, 5445 (1999).
- [24] J. Kondev, Liouville field theory of fluctuating loops, *Physical review letters* **78**, 4320 (1997).
- [25] M. T. Batchelor, J. Suzuki, and C. Yung, Exact results for Hamiltonian walks from the solution of the fully packed loop model on the honeycomb lattice, *Physical review letters* **73**, 2646 (1994).
- [26] E. H. Lieb, Exact solution of the problem of the entropy of two-dimensional ice, *Physical Review Letters* **18**, 692 (1967).
- [27] J. Suzuki, Evaluation of the connectivity of Hamiltonian paths on regular lattices, *Journal of the Physical Society of Japan* **57**, 687 (1988).
- [28] S. Higuchi, Field theoretic approach to the counting problem of Hamiltonian cycles of graphs, *Physical Review E* **58**, 128 (1998).
- [29] J. Kondev, J. de Gier, and B. Nienhuis, Operator spectrum and exact exponents of the fully packed loop model, *Journal of Physics A: Mathematical and General* **29**, 6489 (1996).
- [30] M. Batchelor, H. Blöte, B. Nienhuis, and C. Yung, Critical behaviour of the fully packed loop model on the square lattice, *Journal of Physics A: Mathematical and General* **29**, L399 (1996).
- [31] O. Bodroža-Pantić, H. Kwong, and M. Pantić, Some new characterizations of Hamiltonian cycles in triangular grid graphs, *Discrete Applied Mathematics* **201**, 1 (2016).
- [32] A. Kast, Correlation length and average loop length of the fully packed loop model, *Journal of Physics A: Mathematical and General* **29**, 7041 (1996).
- [33] H. Orland, C. Itzykson, and C. de Dominicis, An evaluation of the number of Hamiltonian paths, *Journal de Physique Lettres* **46**, 353 (1985).
- [34] J. L. Jacobsen and J. Kondev, Field theory of compact polymers on the square lattice, *Nuclear Physics B* **532**, 635 (1998).
- [35] J. Kondev and J. L. Jacobsen, Conformational entropy of compact polymers, *Physical review letters* **81**, 2922 (1998).
- [36] T. Schmalz, G. Hite, and D. Klein, Compact self-avoiding circuits on two-dimensional lattices, *Journal of Physics A: Mathematical and General* **17**, 445 (1984).
- [37] M. Peto, T. Z. Sen, R. L. Jernigan, and A. Kloczkowski, Generation and enumeration of compact conformations on the two-dimensional triangular and three-dimensional fcc lattices, *The Journal of chemical physics* **127**, 07B612 (2007).
- [38] A. V. Melkikh and D. K. Meijer, On a generalized levinthal’s paradox: The role of long-and short range interactions in complex bio-molecular reactions, including protein and dna folding, *Progress in Biophysics and Molecular Biology* **132**, 57 (2018).
- [39] J. Lloyd, S. Biswas, S. H. Simon, S. A. Parameswaran, and F. Flicker, Statistical mechanics of dimers on quasiperiodic ammann-beenker tilings, *Physical Review B* **106**, 094202 (2022).
- [40] B. Grünbaum and G. C. Shephard, *Tilings and Patterns* (W. H. Freeman and Company, New York, 1986).
- [41] R. Ammann, B. Grünbaum, and G. C. Shephard, Aperiodic tiles, *Discrete & Computational Geometry* **8**, 1 (1992).
- [42] M. Baake and U. Grimm, *Aperiodic order*, Vol. 1 (Cambridge University Press, 2013).
- [43] M. Baake and U. Grimm, Mathematical diffraction of aperiodic structures, *Chemical Society Reviews* **41**, 6821 (2012).
- [44] M. Senechal, *Quasicrystals and Geometry* (Cambridge University Press, 1995).
- [45] N. Wang, H. Chen, and K. Kuo, Two-dimensional quasicrystal with eightfold rotational symmetry, *Physical review letters* **59**, 1010 (1987).
- [46] N. Wang, K. K. Fung, and K. H. Kuo, *Appl. Phys. Lett.* **52**, 2120 (1988).
- [47] A. Uri, S. C. de la Barrera, M. T. Randeria, D. Rodan-Legrain, T. Devakul, P. J. D. Crowley, N. Paul, K. Watanabe, T. Taniguchi, R. Lifshitz, L. Fu, R. C. Ashoori, and P. Jarillo-Herrero, Superconductivity and strong interactions in a tunable moiré quasiperiodic crystal, arXiv:2302.00686 [cond-mat.mes-hall] (2023).
- [48] K. Viebahn, M. Sbroscia, E. Carter, J.-C. Yu, and U. Schneider, Matter-wave diffraction from a quasicrystalline optical lattice, *Phys. Rev. Lett.* **122**, 110404 (2019).
- [49] M. Sbroscia, K. Viebahn, E. Carter, J.-C. Yu, A. Gaunt, and U. Schneider, Observing localization in a 2d quasicrystalline optical lattice, *Phys. Rev. Lett.* **125**, 200604 (2020).
- [50] G. M. Sommers, M. J. Gullans, and D. A. Huse, Self-dual quasiperiodic percolation, arXiv:2206.11290 [cond-mat.stat-mech] (2023).
- [51] D. E. Gökmen, S. Biswas, S. D. Huber, Z. Ringel, F. Flicker, and M. Koch-Janusz, Machine learning assisted discovery of exotic criticality in a planar quasicrystal, arXiv:2301.11934 [cond-mat.stat-mech] (2023).
- [52] F. Flicker and J. van Wezel, Quasiperiodicity and 2d topology in 1d charge-ordered materials, *Europhysics Letters* **111**, 37008 (2015).
- [53] F. Flicker and J. van Wezel, Natural 1d quasicrystals from incommensurate charge order, *Physical Review Letters* **115**, 236401 (2015).
- [54] Y. E. Kraus, Y. Lahini, Z. Ringel, M. Verbin, and O. Zeitler, Topological states and adiabatic pumping in

- quasicrystals, *Phys. Rev. Lett.* **109**, 106402 (2012).
- [55] K. A. Madsen, E. J. Bergholtz, and P. W. Brouwer, Topological equivalence of crystal and quasicrystal band structures, *Phys. Rev. B* **88**, 125118 (2013).
- [56] M. Gardner, Mathematical games: About the remarkable similarity between the icosian game and the towers of Hanoi, *Sci. Amer* **196**, 150 (1957).
- [57] J. A. Bondy and V. Chvátal, A method in graph theory, *Discrete Mathematics* **15**, 111 (1976).
- [58] R. W. Robinson and N. C. Wormald, Almost all cubic graphs are Hamiltonian, *Random Structures & Algorithms* **3**, 117 (1992).
- [59] W. T. Tutte, A theorem on planar graphs, *Transactions of the American Mathematical Society* **82**, 99 (1956).
- [60] L. Liu, G. P. T. Choi, and L. Mahadevan, Quasicrystal kirigami, *Phys. Rev. Research* **4**, 033114 (2022).
- [61] F. Flicker, S. H. Simon, and S. Parameswaran, Classical dimers on Penrose tilings, *Physical Review X* **10**, 011005 (2020).
- [62] R. M. Karp, Reducibility among combinatorial problems, in *Complexity of computer computations* (Springer, 1972) pp. 85–103.
- [63] M. R. Garey, Computers and intractability: A guide to the theory of NP-completeness/michael r. garey, david s. johnson, Link (A series of books in the mathematical sciences) (1979).
- [64] R. McGrath, J. Smerdon, H. Sharma, W. Theis, and J. Ledieu, The surface science of quasicrystals, *Journal of Physics: Condensed Matter* **22**, 084022 (2010).
- [65] J.-M. Dubois, New prospects from potential applications of quasicrystalline materials, *Materials Science and Engineering: A* **294**, 4 (2000).
- [66] J. J. Kweon, H.-I. Kim, S.-h. Lee, J. Kim, and S. K. Lee, Quantitative probing of hydrogen environments in quasicrystals by high-resolution nmr spectroscopy, *Acta Materialia* **226**, 117657 (2022).
- [67] R. Diehl, W. Setyawan, and S. Curtarolo, Gas adsorption on quasicrystalline surfaces, *Journal of Physics: Condensed Matter* **20**, 314007 (2008).
- [68] R. J. Baxter, *Exactly solved models in statistical mechanics* (Elsevier, 2016).
- [69] F.-Y. Wu, The Potts model, *Reviews of modern physics* **54**, 235 (1982).
- [70] Y. Hattori, A. Niikura, A. P. Tsai, A. Inoue, T. Masumoto, K. Fukamichi, H. Aruga-Katori, and T. Goto, Spin-glass behaviour of icosahedral mg-gd-zn and mg-tb-zn quasi-crystals, *Journal of Physics: Condensed Matter* **7**, 2313 (1995).
- [71] Z. Islam, I. R. Fisher, J. Zarestky, P. C. Canfield, C. Stassis, and A. I. Goldman, Reinvestigation of long-range magnetic ordering in icosahedral tb-mg-zn, *Phys. Rev. B* **57**, R11047 (1998).
- [72] T. J. Sato, H. Takakura, A. P. Tsai, K. Shibata, K. Ohoyama, and K. H. Andersen, Antiferromagnetic spin correlations in the zn-mg-ho icosahedral quasicrystal, *Phys. Rev. B* **61**, 476 (2000).
- [73] A. Goldman, T. Kong, and A. e. a. Kreyssig, A family of binary magnetic icosahedral quasicrystals based on rare earths and cadmium, *Nature Materials* **12**, 714 (2013).
- [74] R. Tamura, A. Ishikawa, S. Suzuki, T. Kotajima, Y. Tanaka, T. Seki, N. Shibata, T. Yamada, T. Fujii, C.-W. Wang, M. Avdeev, K. Nawa, D. Okuyama, and T. J. Sato, Experimental observation of long-range magnetic order in icosahedral quasicrystals, *Journal of the American Chemical Society* **143**, 19938 (2021), <https://doi.org/10.1021/jacs.1c09954>.
- [75] T. Garel and H. Orland, Mean-field model for protein folding, *Europhysics letters* **6**, 307 (1988).
- [76] T. N. De Silva and V. Sivised, A statistical mechanics perspective for protein folding from q -state potts model, arXiv preprint arXiv:1709.04813 (2017).
- [77] W. T. Tutte and W. T. Tutte, *Graph theory*, Vol. 21 (Cambridge university press, 2001).
- [78] J. A. Bondy, U. S. R. Murty, *et al.*, *Graph theory with applications*, Vol. 290 (Macmillan London, 1976).
- [79] G. Chartrand, *Introductory graph theory* (Courier Corporation, 1977).
- [80] M. Gardner, *Penrose Tiles to Trapdoor Ciphers... and the Return of Dr. Matrix* (The Mathematical Association of America, 1989).
- [81] N. W. Ashcroft and N. D. Mermin, *Solid State Physics* (Harcourt College Publishers, New York, 1976).
- [82] D. B. Shmoys, J. Lenstra, A. R. Kan, and E. L. Lawler, *The traveling salesman problem*, Vol. 12 (John Wiley & Sons, Incorporated, 1985).
- [83] G. Binnig and H. Rohrer, Scanning tunneling microscopy, *Surface science* **126**, 236 (1983).
- [84] P. K. Hansma and J. Tersoff, Scanning tunneling microscopy, *Journal of Applied Physics* **61**, R1 (1987).
- [85] Y. Martin and H. K. Wickramasinghe, Magnetic imaging by “force microscopy” with 1000 Å resolution, *Applied Physics Letters* **50**, 1455 (1987).
- [86] U. Hartmann, Magnetic force microscopy, *Annual review of materials science* **29**, 53 (1999).
- [87] D. Karger, R. Motwani, and G. D. Ramkumar, On approximating the longest path in a graph, *Algorithmica* **18**, 82 (1997).
- [88] J. K. Roberts, *Proc. Roy. Soc. (London)* **A 152**, 469 (1935).
- [89] R. Fowler and G. Rushbrooke, An attempt to extend the statistical theory of perfect solutions, *Transactions of the Faraday Society* **33**, 1272 (1937).
- [90] O. J. Heilmann and E. H. Lieb, Theory of monomer-dimer systems, *Commun. Math. Phys.* **25**, 190 (1972).
- [91] M. R. Garey, D. S. Johnson, and L. Stockmeyer, Some simplified NP-complete problems, in *Proceedings of the sixth annual ACM symposium on Theory of computing* (1974) pp. 47–63.
- [92] P. J. Heawood, Map color theorems, *Quant. J. Math.* **24**, 332 (1890).
- [93] K. Appel and W. Haken, Every planar map is four colorable, *Contemporary Mathematics* **98** (1989).
- [94] T. Sibley and S. Wagon, Rhombic Penrose tilings can be 3-colored, *The American Mathematical Monthly* **107**, 251 (2000).
- [95] V. Beffara and H. Duminil-Copin, The self-dual point of the two-dimensional random-cluster model is critical for $q \geq 1$, *Probability Theory and Related Fields* **153**, 511 (2012).
- [96] W. Selke and D. A. Huse, Interfacial adsorption in planar potts models, *Zeitschrift für Physik B Condensed Matter* **50**, 113 (1983).
- [97] A. D. Sokal and B. Webb, The multivariate Tutte polynomial (alias Potts model), *Surveys in combinatorics* **327**, 173 (2005).
- [98] M. Alford, S. Chandrasekharan, J. Cox, and U.-J. Wiese, Solution of the complex action problem in the Potts model for dense QCD, *Nuclear Physics B* **602**, 61

- (2001).
- [99] F. Graner and J. A. Glazier, Simulation of biological cell sorting using a two-dimensional extended Potts model, *Physical review letters* **69**, 2013 (1992).
- [100] W. G. Wilson and C. A. Vause, Evidence for universality of the Potts model on the two-dimensional Penrose lattice, *Physics Letters A* **126**, 471 (1988).
- [101] G. Xiong, Z.-H. Zhang, and D.-C. Tian, Real-space renormalization group approach to the Potts model on the two-dimensional Penrose tiling, *Physica A: Statistical Mechanics and its Applications* **265**, 547 (1999).
- [102] R. M. Levy, A. Haldane, and W. F. Flynn, Potts hamiltonian models of protein co-variation, free energy landscapes, and evolutionary fitness, *Current opinion in structural biology* **43**, 55 (2017).
- [103] R. B. Potts, Some generalized order-disorder transformations, in *Mathematical proceedings of the cambridge philosophical society*, Vol. 48 (Cambridge University Press, 1952) pp. 106–109.
- [104] J. E. Hopcroft and R. M. Karp, An $n^{5/2}$ algorithm for maximum matchings in bipartite graphs, *SIAM Journal on computing* **2**, 225 (1973).
- [105] N. de Bruijn, Algebraic theory of Penrose’s non-periodic tilings of the plane I, *Indagationes Mathematicae (Proceedings)* **84**, 39 (1981).
- [106] D. Smith, J. S. Myers, C. S. Kaplan, and C. Goodman-Strauss, An aperiodic monotile, arXiv preprint arXiv:2303.10798 (2023).
- [107] D. Smith, J. S. Myers, C. S. Kaplan, and C. Goodman-Strauss, A chiral aperiodic monotile, arXiv preprint arXiv:2305.17743 (2023).
- [108] J. d. Gier, Fully packed loop models on finite geometries, in *Polygons, Polyominoes and Polycubes* (Springer, 2009) pp. 317–346.
- [109] L. Onsager, Crystal statistics. I. a two-dimensional model with an order-disorder transition, *Physical Review* **65**, 117 (1944).
- [110] R. P. Feynman, *Statistical mechanics: a set of lectures* (CRC press, 2018).
- [111] E. H. Lieb, Two theorems on the hubbard model, *Phys. Rev. Lett.* **62**, 1201 (1989).
- [112] R. Bhola, S. Biswas, M. M. Islam, and K. Damle, Dulmage-mendelsohn percolation: Geometry of maximally packed dimer models and topologically protected zero modes on site-diluted bipartite lattices, *Phys. Rev. X* **12**, 021058 (2022).
- [113] M. Kohmoto and B. Sutherland, Electronic states on a penrose lattice, *Phys. Rev. Lett.* **56**, 2740 (1986).
- [114] A. Koga and H. Tsunetsugu, Antiferromagnetic order in the hubbard model on the penrose lattice, *Physical Review B* **96**, 214402 (2017).
- [115] E. Day-Roberts, R. M. Fernandes, and A. Kamenev, Nature of protected zero-energy states in penrose quasicrystals, *Phys. Rev. B* **102**, 064210 (2020).
- [116] A. Koga, Superlattice structure in the antiferromagnetically ordered state in the hubbard model on the ammann-beenker tiling, *Phys. Rev. B* **102**, 115125 (2020).
- [117] B. Sutherland, Localization of electronic wave functions due to local topology, *Phys. Rev. B* **34**, 5208 (1986).
- [118] J. Schirmann, S. Franca, F. Flicker, and A. G. Grushin, Physical properties of the hat aperiodic monotile: Graphene-like features, chirality and zero-modes, arXiv:2307.11054 (2023).
- cond – mat.mes – hall*
- [119] P. Baniasadi, V. Ejov, J. A. Filar, M. Haythorpe, and S. Rossomakhine, Deterministic “snakes and ladders” heuristic for the hamiltonian cycle problem, *Mathematical Programming Computation* **6**, 55 (2014).
- [120] P. Baniasadi, V. Ejov, M. Haythorpe, and S. Rossomakhine, A new benchmark set for traveling salesman problem and hamiltonian cycle problem, arXiv preprint arXiv:1806.09285 (2018).
- [121] J. Slegers and D. van den Berg, The hardest hamiltonian cycle problem instances: the plateau of yes and the cliff of no, *SN Computer Science* **3**, 372 (2022).
- [122] K. Helsgaun, An effective implementation of the linkernighan traveling salesman heuristic, *European journal of operational research* **126**, 106 (2000).
- [123] D. L. Applegate, R. E. Bixby, V. Chvátal, and W. J. Cook, The traveling salesman problem, in *The Traveling Salesman Problem* (Princeton university press, 2011).
- [124] F. L. Metz, I. Neri, and T. Rogers, Spectral theory of sparse non-hermitian random matrices, *Journal of Physics A: Mathematical and Theoretical* **52**, 434003 (2019).
- [125] P. Webley and D. Danaci, Co2 capture by adsorption processes, in *Carbon Capture and Storage*, RSC Energy and Environment Series No. 26, edited by M. Bui and N. Dowell (The Royal Society of Chemistry, United Kingdom, 2020) pp. 106–167, 26th ed.
- [126] D. Louzguine-Luzgin and A. Inoue, Formation and properties of quasicrystals, *Annual Review of Materials Research* **38**, 403 (2008).
- [127] Z. Papadopolos, G. Kasner, J. Ledieu, E. J. Cox, N. V. Richardson, Q. Chen, R. D. Diehl, T. A. Lograsso, A. R. Ross, and R. McGrath, Bulk termination of the quasicrystalline fivefold surface of $\text{al}_{70}\text{pd}_{21}\text{mn}_9$, *Phys. Rev. B* **66**, 184207 (2002).
- [128] Z. Papadopolos, P. Pleasants, G. Kasner, V. Fournée, C. J. Jenks, J. Ledieu, and R. McGrath, Maximum density rule for bulk terminations of quasicrystals, *Phys. Rev. B* **69**, 224201 (2004).
- [129] R. McGrath, J. Ledieu, E. J. Cox, and R. D. Diehl, Quasicrystal surfaces: structure and potential as templates, *Journal of Physics: Condensed Matter* **14**, R119 (2002).
- [130] R. McGrath, J. A. Smerdon, H. R. Sharma, W. Theis, and R. Ledieu, The surface science of quasicrystals, *Journal of Physics: Condensed Matter* **22**, 084022 (2010).
- [131] M. Pagliaro, C. Della Pina, F. Mauriello, and R. Ciriminna, Catalysis with silver: From complexes and nanoparticles to morals and single-atom catalysts, *Catalysts* **10**, 1343 (2020).
- [132] D. A. Rabson, N. D. Mermin, D. S. Rokhsar, and D. C. Wright, *Reviews of Modern Physics* **63** (1991).
- [133] E. Cockayne and S. Hedetniemi, Optimal domination in graphs, *IEEE Transactions on circuits and systems* **22**, 855 (1975).
- [134] E. J. Cockayne and S. T. Hedetniemi, Towards a theory of domination in graphs, *Networks* **7**, 247 (1977).
- [135] U. Feige, M. M. Halldórsson, and G. Kortsarz, Approximating the domatic number, in *Proceedings of the Thirty-Second Annual ACM Symposium on Theory of Computing* (2000) pp. 134–143.

- [136] R. Yuster, The domatic number of regular and almost regular graphs, arXiv preprint math/0111257 (2001).
- [137] M. Yannakakis, The node deletion problem for hereditary properties, Computer Science Laboratory, Princeton University, Princeton, NJ. (A1.2) **Report No. TR-240** (1978a).

Appendix A: Detailed Figures

In this appendix we include detailed figures to accompany the proof sections in the main text. Fig. A.1 and Fig. A.2 show intermediate steps for obtaining the Hamiltonian cycle in Fig. 6. In Fig. A.1, black e_0 edges form loops visiting every $8_{n<0}$ -vertex (i.e. every vertex which is not an 8-vertex). We placed red e_1 edges along the e_1 -loops (red loops in Fig. 5) to add 8_0 -vertices onto the loops. After this we also placed blue e_2 edges along the e_2 -loop (blue loop in Fig. 5), with one corner folded, to

add the central vertex and 8_1 -vertices onto the loops. Note that some parts of the blue e_2 edges overlaps with the red e_1 edges. Noting that augmentation of a set of edges is reversed by a second augmentation of the same set of edges, in Fig. A.2 these overlapping e_2 edges and e_1 edges will augment to leave the L_0 tiling unchanged. Hence we can remove these overlapping edges completely. This results in a rewiring of e_1 -loops and the e_2 -loop into a single loop as shown. Augmenting this single loop, consisting of the remaining red and blue edges, will give us the Hamiltonian cycle shown in Fig. 6.

Fig. A.3 is a bigger version of Fig. 8, showing a solution for the 3-colouring problem on a large patch of AB tiling resulting by placing tile 1 and tile 2 shown in Fig. 7, and colouring the remaining ladders consistently on the basis of colors of their surrounding rhombuses such that no two adjacent faces share a colour.

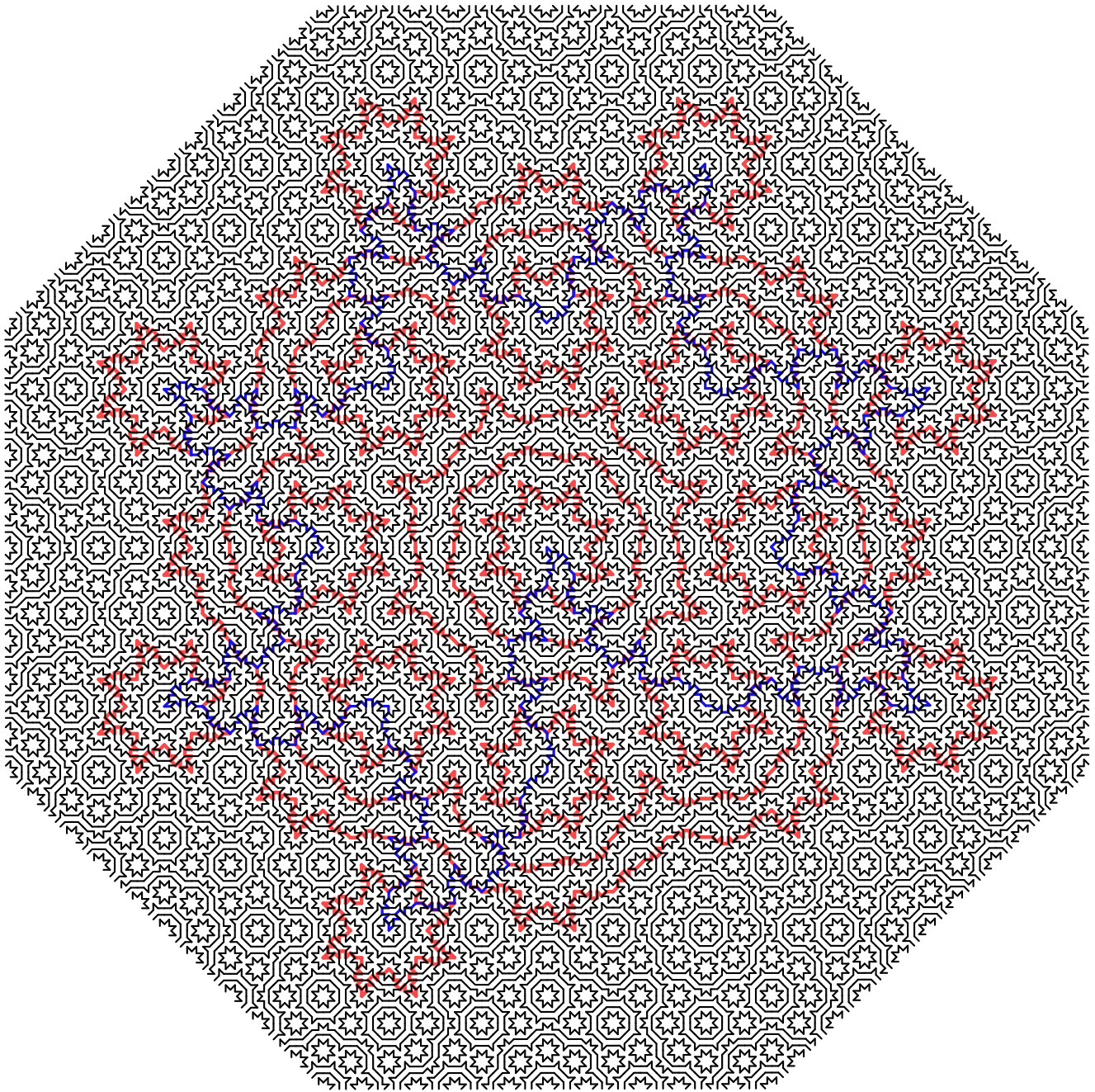


FIG. A.1: The canonical placement of e_0 edges (black) form loops visiting every $8_{n<0}$ -vertex (i.e. every vertex which is not an 8-vertex). Now e_1 edges (red) are placed along the e_1 -loops (see Fig. 5) to add 8_0 -vertices onto the loops. Further e_2 edges (blue) are placed along the e_2 -loop, with one corner folded, to add the central vertex and 8_1 -vertices onto the loops. Note that some parts of the blue e_2 edges overlaps with the red e_1 edges. This process can be iterated to any order.

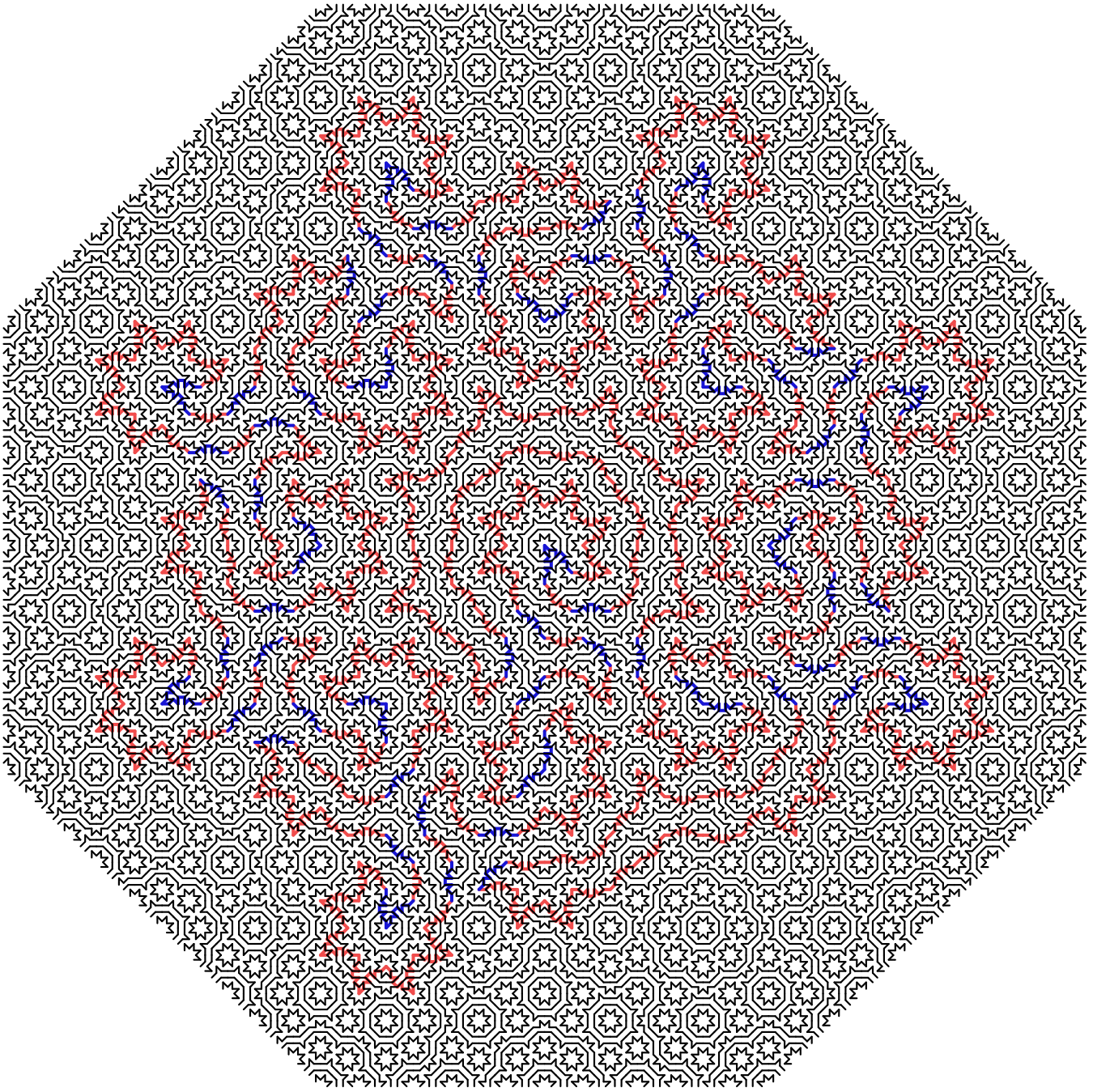


FIG. A.2: The overlapping e_2 edges and e_1 edges as shown in Fig A.1 will augment to leave the L_0 tiling unchanged. Hence we can remove these overlapping e_2 edges and e_1 edges completely. This results in the rewiring of e_1 -loops and the e_2 -loop into a single loop as shown here. Finally augmenting this single loop, consisting of the remaining red and blue edges, will give the Hamiltonian cycle shown in Fig. 6.

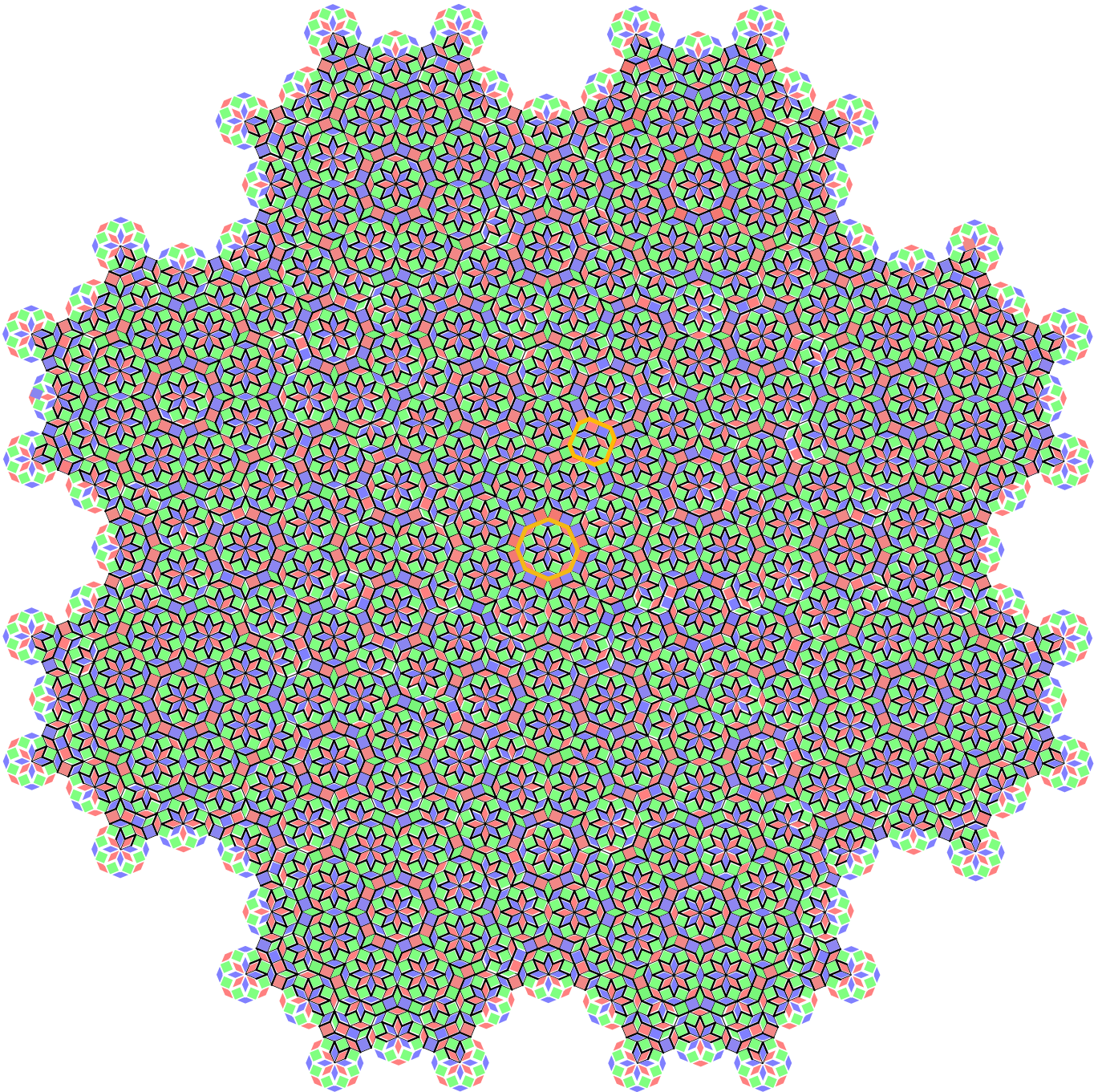


FIG. A.3: The 3-coloured AB tiling using tile 1 and tile 2 (both outlined in gold) as mentioned in Sec. IV C.

Appendix B: Solutions to other non-trivial problems on AB

1. The Minimum Dominating Set Problem

A dominating set D of a graph G is a subset of the vertices of G such that all the vertices not in D are adjacent to at least one vertex in D . The minimum dominating set (MDS) is a dominating set containing the fewest possible vertices; its cardinality is called the domination number, $\gamma(G)$.

Problem statement [63]: given a graph G and integer k , is the domination number $\gamma(G) \leq k$? The corresponding optimisation problem is to find the MDS.

Solution: if G is built from N copies of $L_{1/2}$ tiles, yes iff $N \leq k$.

Proof: Fig. 2 shows the single-inflation rules for the rhombus and square, level $L_{1/2}$. The set of red vertices forms an MDS for all vertices within each $L_{1/2}$ tile. Since these inflated tiles cover the entire tiling (owing to discrete scale symmetry), the union of minimum dominating sets of all these inflated tiles must be a dominating set for any patch of the AB tiling, or the tiling itself in the thermodynamic limit. That this is actually an MDS can be seen from the fact that there is no redundancy in the placement of the red vertices in Fig. 2: no red vertex has another red as a neighbour, which implies that the set constitutes an MDS for the whole AB tiling. A larger region of the MDS is shown in Fig. B.1. Note that the MDS is not unique.

Comment: the proof relies only on the discrete scale symmetry of AB tilings, without reference to the Hamiltonian cycle construction. In Section B 2 we will combine this MDS solution with the Hamiltonian cycle construction to solve a different problem.

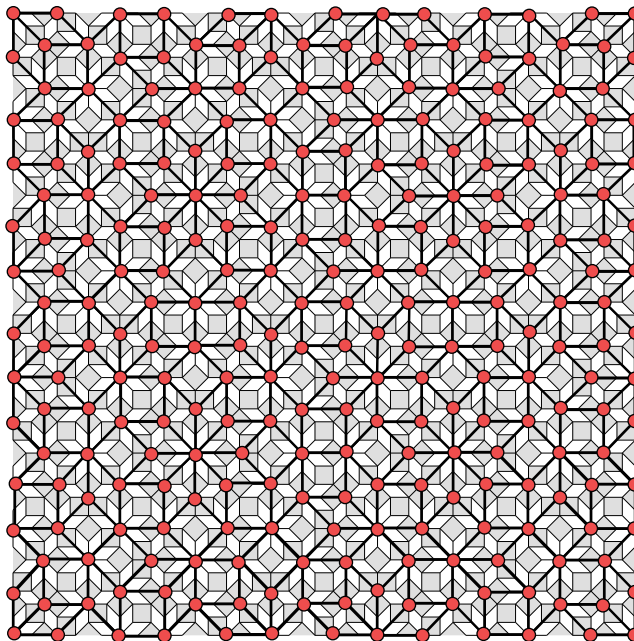


FIG. B.1: A portion of AB tiling showing the minimum dominating set vertices (red), which as proved in Section B 1 are also vertices of single inflated tiles.

2. The Domatic Number Problem

The domatic number $d(G)$ for any given graph G with a set of vertices V is the maximum number of disjoint dominating sets into which V can be partitioned.

Problem statement [133]: for a given graph G and integer k , does G have a domatic number $d(G) \geq k$? The corresponding optimisation problem is to find the domatic number and a maximum sized partition of V into dominating sets.

Solution: if $G = \text{AB}$, yes iff $k \leq 3$.

Proof: first we use known results to prove that (i) $2 \leq d(G) < 4$. Next we use our Hamiltonian cycles to construct three disjoint dominating sets, proving (ii) $d(G) > 2$, and hence $d(G) = 3$.

(i) The domatic number concept was introduced in Ref. 134, where it was proven that for any graph G , $d(G) \leq \lambda + 1$, where λ is the minimum degree of the graph. Furthermore, if G contains no isolated vertices, then $d(G) \geq 2$ [135]. Together, these statements imply that for the AB tiling (with $\lambda = 3$), the domatic number must be $2 \leq d(G) \leq 4$. If we know the domination number $\gamma(G)$ for any graph G , it follows that [136]:

$$d(G) \leq \frac{|G|}{\gamma(G)}. \quad (\text{B1})$$

Denote H the patch of the AB tiling shown in Fig. B.3(a), which is a once-inflated 8-vertex. The vertices shown in

red form its MDS as shown in Section B 1. In this patch, $\gamma(H) = 17$ and $|H| = 57$, and so

$$d(H) \leq 3.35. \tag{B2}$$

Therefore $d(H) < 4$. Since $H \subset G = AB$, it follows that $d(G) < 4$.

(ii) The results so far show that $2 \leq d(G) \leq 3$. Finding a partition of the vertices V of G into three disjoint dominating sets therefore suffices to prove that $d(G) = 3$ for the entire AB tiling. We do this using the FPLs on AB^* we constructed in Sec. III A. These loops take two forms: they either appear as 16-vertex ‘stars’ encircling 8-vertices, or they appear as concentric pairs which we envisage as the rails of the ‘ladder’ of tiles they bound.

Let $V = \{V_1, V_2, V_3\}$ be the partition of the vertices V of G into three disjoint dominating sets, which we colour red, blue and yellow respectively. In this way, we seek a colouring of vertices such that every vertex in V will have at least one neighbour of each color. Note that the restriction to finding minimal sets is dropped, so that a colour can have a neighbour of the same colour.

We can take V_1 to be the minimum dominating set we found in Section B 1. Take two units of the ladders as shown in Fig. B.3(b) with vertices coloured as shown. Red vertices are on the same sites as of the MDS found in Sec. B 1, while blue and yellow vertices are placed such that every vertex in both units of ladder, except those circled, have at least one neighbour of each colour. In Fig. B.3(c) we denote ladder segments either green or purple. The purple unit of the ladder will always appear with a neighbouring green structure, providing the required red neighbour to the circled vertices.

Ref. 39 demonstrated that these two units can form ladders of any order over the entire tiling. Hence repeating these two units with the specified vertex colour arrangements shows that all the vertices over any ladder of the tiling will have at least one neighbour of each colour. For this specific arrangement of three colours, joining two ladder units causes the red and yellow vertices on each of their ends to overlap consistently. Using the blue and yellow arrangements on the star loop shown in Fig. B.3(d), filling the entire tiling using the loops and ladder units of Figs. B.3(b), (c) and (d) results in Fig. B.3(e). All the vertices of the entire AB tiling now have at least one neighbour of each colour; AB is hence divided into three disjoint dominating sets denoted by the three colors, as required. Note that all 8-vertices are in the MDS of Sec. B 1), and hence are coloured red.

3. The Induced Path Problem

An induced path in an undirected graph G is a sequence of vertices such that a pair of vertices is adjacent in the sequence iff the vertices have an edge in G . An induced cycle is an induced path which closes.

Problem statement [63, 137]: for a graph G and a positive integer k , does G contain an induced cycle of length at least k ? The corresponding optimisation problem is to find an induced cycle of length k .

Solution: yes, if $G = AB$.

Proof: in this case it is convenient to consider the D_8 -symmetric regions W_n . Fig. B.2 shows the loops of the FPL on AB^* constructed in Sec. III A. We see that any non adjacent vertices on these loops do not have an edge in G , while any adjacent vertices do. Hence these loops are induced cycles. The longest such loop in W_n is of length $8(9^n + 1)$ (this can be proven using the inflation rules of Fig. 2). Since any AB tiling contains W_∞ , the answer to the problem is ‘yes’ for any k , finite or infinite.

Comments: on general graphs the problem remains NPC if an induced path is sought rather than an induced cycle. That problem can also be solved on AB, by deleting any pair of consecutive edges along the cycle. Longer induced cycles than those we consider can be found in W_n , but the problem statement does not require them.

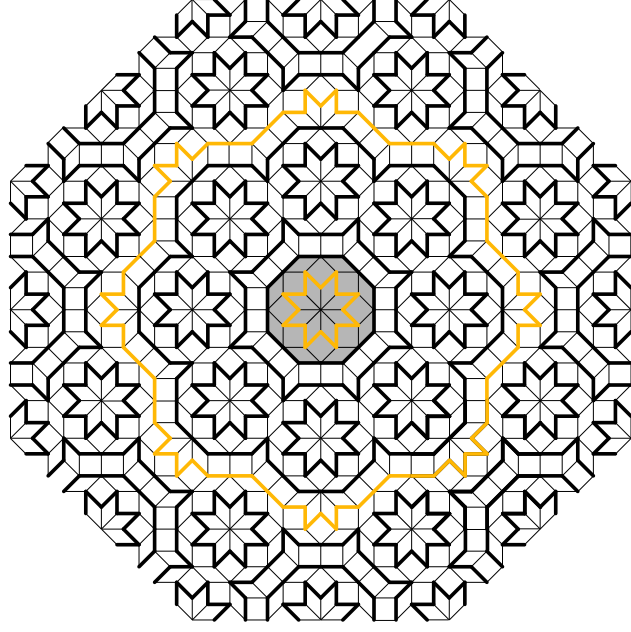


FIG. B.2: FPLs on AB^* formed by the method in Section III A form induced paths on AB. The longest induced path in region W_n created by this method is of length $8(9^n + 1)$. The total region shown here is W_1 , with W_0 highlighted in grey. The corresponding induced paths are shown in gold.

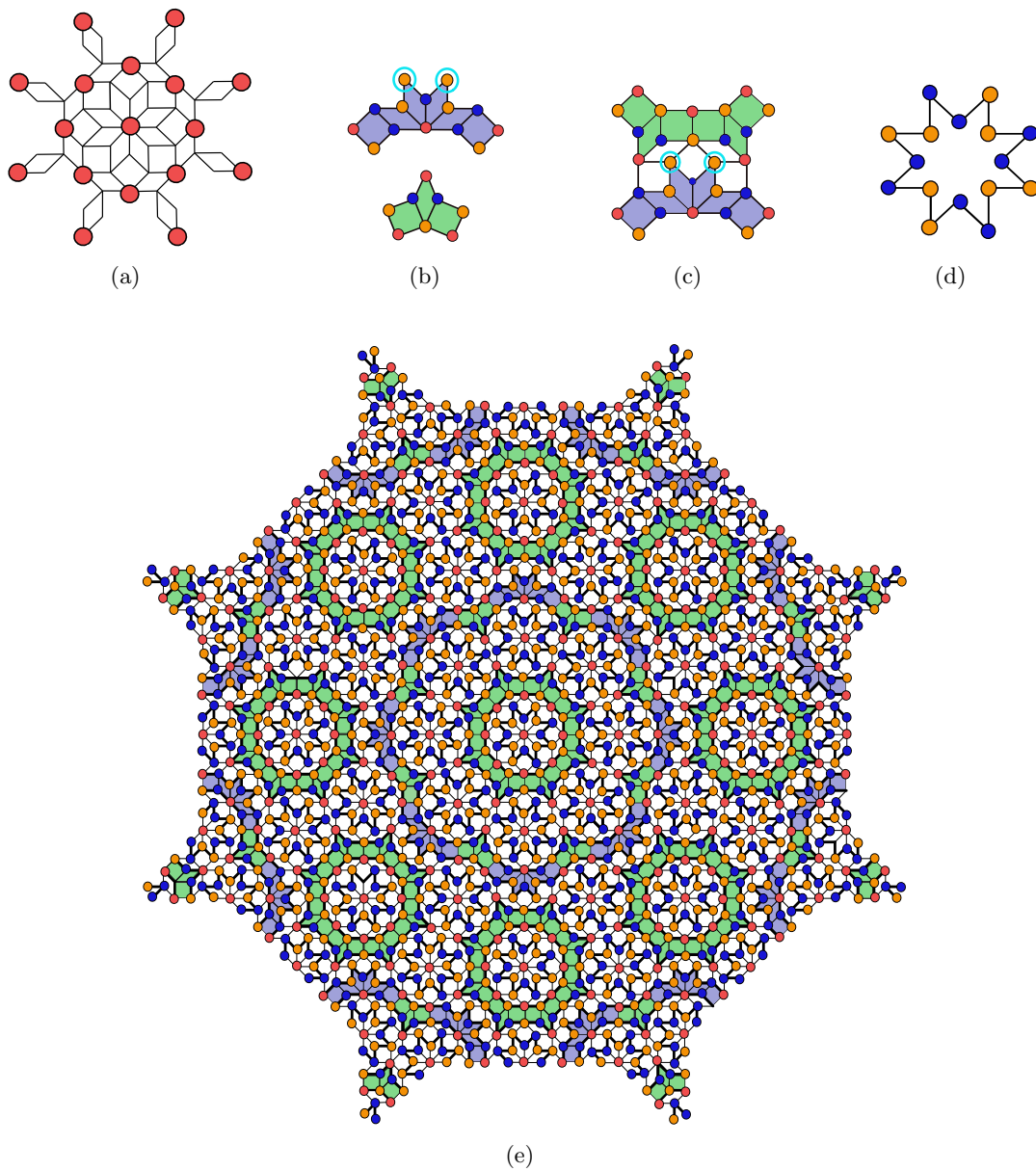


FIG. B.3: (a) The once-inflated 8-vertex, with a dominating set shown in red. (b) Two units of ‘ladders’ (purple and green) which can be used to construct ladders of any order. All vertices on both ladders, except those circled, are partitioned into three disjoint dominating sets shown in three colours (red, blue and yellow). (c) The purple ladder unit always appears with two green unit ladder units above, hence providing the required red neighbour to the circled vertices. (d) The vertex partition required for the ‘star’ configuration. (e) A partition of AB into three disjoint sets obtained by combining loops and ladders from (b),(c), and (d). Note that red vertices are the MDS constructed in Sec. B 1.